



Fine-particle water and pH in the southeastern United States

H. Guo¹, L. Xu², A. Bougiatioti^{2,8}, K. M. Cerully^{2,*}, S. L. Capps^{4,**}, J. R. Hite Jr.¹, A. G. Carlton⁵, S.-H. Lee⁶, M. H. Bergin^{1,3}, N. L. Ng^{1,2}, A. Nenes^{1,2,7}, and R. J. Weber¹

¹School of Earth and Atmospheric Sciences, Georgia Institute of Technology, Atlanta, GA, USA

²School of Chemical and Biomolecular Engineering, Georgia Institute of Technology, Atlanta, GA, USA

³School of Civil and Environmental Engineering, Georgia Institute of Technology, Atlanta, GA, USA

⁴Office of Research and Development, United States Environmental Protection Agency, Research Triangle Park, NC, USA

⁵Department of Environmental Sciences, Rutgers University, New Brunswick, NJ, USA

⁶College of Public Health, Kent State University, Kent, OH, USA

⁷Foundation for Research and Technology, Hellas, Greece

⁸National Technical University of Athens, Athens, Greece

* now at: TSI, Inc., Shoreview, MN, USA

** now at: Department of Mechanical Engineering, University of Colorado Boulder, Boulder, CO, USA

Correspondence to: R. J. Weber (rodney.weber@eas.gatech.edu) and A. Nenes (athanasios.nenes@gatech.edu)

Received: 30 August 2014 – Published in Atmos. Chem. Phys. Discuss.: 29 October 2014

Revised: 6 April 2015 – Accepted: 17 April 2015 – Published: 11 May 2015

Abstract. Particle water and pH are predicted using meteorological observations (relative humidity (RH), temperature (T)), gas/particle composition, and thermodynamic modeling (ISORROPIA-II). A comprehensive uncertainty analysis is included, and the model is validated. We investigate mass concentrations of particle water and related particle pH for ambient fine-mode aerosols sampled in a relatively remote Alabama forest during the Southern Oxidant and Aerosol Study (SOAS) in summer and at various sites in the southeastern US during different seasons, as part of the Southeastern Center for Air Pollution and Epidemiology (SCAPE) study. Particle water and pH are closely linked; pH is a measure of the particle H^+ aqueous concentration and depends on both the presence of ions and amount of particle liquid water. Levels of particle water, in turn, are determined through water uptake by both the ionic species and organic compounds. Thermodynamic calculations based on measured ion concentrations can predict both pH and liquid water but may be biased since contributions of organic species to liquid water are not considered. In this study, contributions of both the inorganic and organic fractions to aerosol liquid water were considered, and predictions were in good agreement with measured liquid water based on differences in ambient and dry light scattering coefficients (prediction vs. measurement: slope = 0.91, intercept = $0.5 \mu\text{g m}^{-3}$,

$R^2 = 0.75$). ISORROPIA-II predictions were confirmed by good agreement between predicted and measured ammonia concentrations (slope = 1.07, intercept = $-0.12 \mu\text{g m}^{-3}$, $R^2 = 0.76$). Based on this study, organic species on average contributed 35 % to the total water, with a substantially higher contribution (50 %) at night. However, not including contributions of organic water had a minor effect on pH (changes pH by 0.15 to 0.23 units), suggesting that predicted pH without consideration of organic water could be sufficient for the purposes of aqueous secondary organic aerosol (SOA) chemistry. The mean pH predicted in the Alabama forest (SOAS) was 0.94 ± 0.59 (median 0.93). pH diurnal trends followed liquid water and were driven mainly by variability in RH; during SOAS nighttime pH was near 1.5, while daytime pH was near 0.5. pH ranged from 0.5 to 2 in summer and 1 to 3 in the winter at other sites. The systematically low pH levels in the southeast may have important ramifications, such as significantly influencing acid-catalyzed reactions, gas–aerosol partitioning, and mobilization of redox metals and minerals. Particle ion balances or molar ratios, often used to infer pH, do not consider the dissociation state of individual ions or particle liquid water levels and do not correlate with particle pH.

1 Introduction

The concentration of the hydronium ion (H^+) in aqueous aerosols, or pH, is an important aerosol property that drives many processes related to particle composition and gas–aerosol partitioning (Jang et al., 2002; Meskhidze et al., 2003; Gao et al., 2004; Iinuma et al., 2004; Tolocka et al., 2004; Edney et al., 2005; Czoschke and Jang, 2006; Kleindienst et al., 2006; Surratt et al., 2007; Eddingsaas et al., 2010; Surratt et al., 2010). Measurement of pH is highly challenging, and so indirect proxies are often used to represent particle acidity. The most common is an ion balance: the charge balance of measurable cations and anions (excluding the hydronium ion). Although correlated with an acidic (net negative balance) or alkaline (net positive balance) aerosol (Surratt et al., 2007; Tanner et al., 2009; Pathak et al., 2011; Yin et al., 2014), an ion balance cannot be used as a measure of the aerosol concentration of H^+ in air (i.e., moles H^+ per volume of air, denoted hereafter as H_{air}^+). This is due to two factors: first, an ion balance assumes all ions are completely dissociated, but multiple forms are possible, depending on pH (e.g., sulfate can be in the form of H_2SO_4 , HSO_4^- , or SO_4^{2-}); second, pH depends on the particle liquid water content (LWC), as pH is the concentration of H^+ in an aqueous solution. LWC can vary considerably over the course of a day and between seasons, significantly influencing pH (Seinfeld and Pandis, 2006). Aerosol thermodynamic models, such as ISORROPIA-II (Nenes et al., 1998; Fountoukis and Nenes, 2007) and E-AIM (Clegg et al., 1998), are able to calculate LWC and particle pH – based on concentrations of various aerosol species, temperature (T), and relative humidity (RH) – and offer a more rigorous approach to obtain aerosol pH (Pye et al., 2013). ISORROPIA-II calculates the composition and phase state of an $\text{NH}_4^+ - \text{SO}_4^{2-} - \text{NO}_3^- - \text{Cl}^- - \text{Na}^+ - \text{Ca}^{2+} - \text{K}^+ - \text{Mg}^{2+}$ –water inorganic aerosol in thermodynamic equilibrium with water vapor and gas-phase precursors. The model has been tested with ambient data to predict acidic or basic compounds, such as $\text{NH}_3(\text{g})$, NH_4^+ , and NO_3^- (Meskhidze et al., 2003; Nowak et al., 2006; Fountoukis et al., 2009; Hennigan et al., 2015).

LWC is a function of RH, particle concentration, and composition, and it is the most abundant particle-phase species in the atmosphere, at least 2–3 times the total aerosol dry mass on a global average (Pilinis et al., 1995; Liao and Seinfeld, 2005). At 90 % RH, the scattering cross section of an ammonium sulfate particle can increase by a factor of 5 or more above that of the dry particle, due to large increases in size from water uptake (Malm and Day, 2001). Because of this, LWC is the most important contributor to direct radiative cooling by aerosols (Pilinis et al., 1995), currently thought to be -0.45 W m^{-2} (-0.95 to $+0.05 \text{ W m}^{-2}$) (IPCC, 2013). LWC plays a large role in secondary aerosol formation for inorganic and possibly organic species by providing a large aqueous surface for increased gas uptake and a liquid

phase where aqueous-phase chemical reactions can result in products of lower vapor pressures than the absorbed gases (Seinfeld and Pandis, 2006; Ervens et al., 2011; Nguyen et al., 2013). In the eastern USA, it has been suggested that the potential for organic gases to partition to LWC is greater than the potential to partition to particle-phase organic matter (Carlton and Turpin, 2013), and partitioning of water-soluble organic carbon (WSOC) into the particle phase becomes stronger as RH (i.e., LWC) increases (Hennigan et al., 2008). Thus LWC enhances particle scattering effects directly by increasing particle cross sections (Nemesure et al., 1995) and indirectly by promoting secondary aerosol formation (Ervens et al., 2011; Nguyen et al., 2013).

The behavior of inorganic salts under variable RH is well established both experimentally and theoretically. It is known that dry inorganic salts (or mixtures thereof) exhibit a phase change, called deliquescence, when exposed to RH above a characteristic value. During deliquescence, the dry aerosol spontaneously transforms (at least partially) into an aqueous solution (Tang, 1976; Wexler and Seinfeld, 1991; Tang and Munkelwitz, 1993). In contrast, due to its chemical complexity that evolves with atmospheric aging, the relationship of organics to LWC is not well characterized and requires a parameterized approach (Petters and Kreidenweis, 2007). Relationships between volatility, oxidation level, and hygroscopicity are not always straightforward and still remain to be fully understood (Frosch et al., 2011; Villani et al., 2013; Cerully et al., 2014; Hildebrandt Ruiz et al., 2014). Despite the abundance and importance of LWC, it is not routinely measured. Thus typically, particle total mass concentration (that includes liquid water) is often not characterized. In general, LWC is measured by perturbing the in situ RH. The loss of particle volume when RH is lowered is assumed to be solely due to evaporated water. Approaches for LWC measurements are classified into single-particle-size probes and bulk size quantification (Sorooshian et al., 2008). Single-particle-size probes provide more information, i.e., size-resolved hygroscopic growth, and usually tend to be slow due to whole size range scanning. In contrast, bulk size measurements quantify the total water amount directly. The LWC measurement presented in this paper by nephelometers is a bulk measurement.

As part of the Southern Oxidant and Aerosol Study (SOAS), we made detailed measurements of particle organic and inorganic composition (Xu et al., 2015), and aerosol hygroscopicity (Cerully et al., 2014), and indirect measurements of particle LWC. These data are used to first determine the particle water mass concentrations, which are then utilized in a thermodynamic model for predicting pH. The fine-particle LWC and pH data from this analysis are used in our other studies of secondary aerosol formation as part of SOAS and discussed in companion papers to this work (Cerully et al., 2014; Xu et al., 2015).

2 Data collection

2.1 Measurement sites

Aerosol measurements were conducted at the Southeastern Aerosol Research and Characterization (SEARCH) Centreville site (CTR; 32.90289° N, 87.24968° W; altitude: 126 m), located in Brent, Alabama, as part of SOAS (<http://soas2013.rutgers.edu>). SOAS ground measurements were made from 1 June to 15 July in the summer of 2013. CTR is a rural site within a large forested region dominated by biogenic volatile organic compound (VOC) emissions, with minor local anthropogenic emissions and some plumes transported from other locations (coal-fired electrical generating units, urban emissions, biomass burning, mineral dust). It is representative of background conditions in the southeastern US and chosen to investigate biogenic secondary organic aerosol (SOA) formation and its interaction with anthropogenic pollution transported from other locations.

Additional measurements were also made at various sampling sites in and around the metropolitan Atlanta region from May 2012 to December 2012 as part of a large health study: the Southeastern Center for Air Pollution and Epidemiology (SCAPE). A map of all five sites is shown in Fig. 1. The SCAPE measurement sites include

1. a road-side (RS) site (33.775602° N, 84.390957° W), situated within 5 m from the interstate highway (I75/85) in midtown Atlanta and chosen to capture fresh traffic emissions;
2. a near-road site (GIT site, 33.779125° N, 84.395797° W), located on the rooftop of the Ford Environmental Science and Technology (EST) building at Georgia Institute of Technology (GIT), Atlanta, roughly 30 to 40 m above ground level, 840 m from the RS site;
3. Jefferson Street (JST) (33.777501° N, 84.416667° W), a central SEARCH site representative of the Atlanta urban environment, located approximately 2000 m west of the GIT site;
4. Yorkville (YRK) (33.928528° N, 85.045483° W), the rural SEARCH pair of JST, situated in an agricultural region approximately 70 km west from the JST, GIT, and RS sites.

More information on the SEARCH sites can be found elsewhere (Hansen et al., 2003; Hansen et al., 2006). We first focus on the SOAS campaign data, where a wide range of instrumentation was deployed (<http://soas2013.rutgers.edu>) to develop a comprehensive method of predicting LWC and pH, as well as assessing their uncertainties. The approach is then applied to the SCAPE site data to provide a broader spatial and temporal assessment of PM_{2.5} pH in the southeastern US.

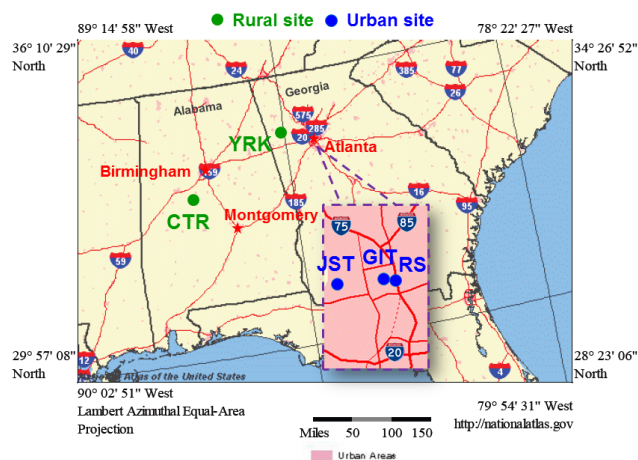


Figure 1. Sampling sites in the southeastern USA, consisting of two rural and three urban sites.

2.2 Instrumentation

2.2.1 PILS-IC

PM_{2.5} or PM₁ (particles with aerodynamic diameters < 2.5 or 1.0 μm at ambient conditions) water-soluble ions were measured by a particle-into-liquid sampler coupled to an ion chromatograph (PILS-IC; Metrohm 761 Compact IC). Similar setups are described in previous field studies (Orsini et al., 2003; Liu et al., 2012). Metrosep A Supp-5, 150/4.0 anion column and C 4, 150/4.0 cation column (Metrohm USA, Riverside, FL) were used to separate the PILS liquid sample anions (sulfate, nitrate, chloride, oxalate, acetate, formate) and cations (ammonium, sodium, potassium, calcium, magnesium) at a 20 min duty cycle. The PILS sample ambient air flow rate was 16.8 ± 0.4 L min⁻¹. URG (Chapel Hill, NC) cyclones were used to provide PM cut sizes of PM_{2.5} for the first half of field study (1 June to 22 June) and PM₁ for the latter half (23 June to 15 July). Honeycomb acid (phosphoric acid)- and base (sodium carbonate)-coated denuders removed interfering gases before entering the PILS. The sample inlet was ~ 7 m above ground level and ~ 4 m long. The sampling line was insulated inside the trailer (typical indoor *T* was 25 °C) and less than 1 m in length to minimize possible changes in aerosol composition prior to measurement. Periodic 1 h blank measurements were made every day by placing a HEPA filter (Pall Corp.) on the cyclone inlet. All data were blank-corrected. The PILS IC was only deployed for the SOAS study.

2.2.2 AMS

A high-resolution time-of-flight aerosol mass spectrometer (HR-ToF-AMS, Aerodyne Research Inc., hereafter referred to as “AMS”) provided real-time, quantitative measurements of the non-refractory components of submicron aerosols (DeCarlo et al., 2006; Canagaratna et al., 2007). In brief, par-

ticles were first dried (RH < 20 %) and then immediately sampled through an aerodynamic lens into the high vacuum region of the mass spectrometer, then transmitted into a detection chamber where particles impact on a hot surface (600 °C). Non-refractory species are flash-vaporized and then ionized by 70 eV electron impact ionization. The generated ions are extracted into the time-of-flight mass spectrometer. Further details on the AMS setup and data processing can be found in Xu et al. (2015).

2.2.3 CCNc

The particle hygroscopic parameter, κ (Petters and Kreidenweis, 2007), used to infer the hygroscopic properties (liquid water associated with organics), was obtained from size-resolved CCN measurements from a Droplet Measurement Technologies continuous-flow streamwise thermal gradient cloud condensation nuclei counter (CFSTGC, referred to hereafter as CCNc) (Roberts and Nenes, 2005; Lance et al., 2006). The CCNc exposes aerosols to a known supersaturation and then counts the activated particles that grow rapidly to droplet size. Köhler theory can be used to parameterize the water-phase properties (here, expressed by κ ; Petters and Kreidenweis, 2007) of the organic aerosol, based on the size of particles that form CCN and their composition. A URG (Chapel Hill, NC) PM₁ cyclone was installed for both AMS and CCNc. The details of the CCNc setup and data analysis procedure can be found in Cerully et al. (2014).

2.2.4 Ambient vs. dry nephelometers

PM_{2.5} (URG cyclones) aerosol light scattering coefficients (σ_{sp}) were measured online with two different nephelometers (Radiance Research M903) to infer LWC. Both were operated at nominally 3 L min⁻¹. Particle dry scattering was measured with a nephelometer located in the air-conditioned sampling trailer operated with a nafion dryer upstream that maintained an RH of 32 ± 2 % (study mean ± SD, $n = 12\,464$ based on 5 min averages). The other was situated in a small white three-sided wooden shelter (one side covered by a loose tarp) located a distance away from all buildings to provide a scattering measurement at ambient T and RH. Both PM_{2.5} cut cyclones were located in ambient conditions, and both nephelometers were calibrated by CO₂ prior to the SOAS field campaign. Typical uncertainty is 3 % for scattering coefficients (Mitchell et al., 2009). In addition, the nephelometer RH sensors were calibrated by placing the sensors in a closed container above aqueous saturated salt solutions that had reached equilibrium (measurements made in a thermally insulated container after a period of a few hours). Solution temperatures were monitored. Details on the calibration results are provided in the Supplement Sect. 1. Recorded RH was corrected by the calibration results.

The deployment status of the above instruments at the SOAS and SCAPE sites are summarized in Table 1.

2.3 Determining LWC from nephelometers

Particle water was inferred from the ratio of ambient and dry PM_{2.5} scattering coefficients (σ_{sp}) measured by the two nephelometers (defined here as aerosol hygroscopic growth factor, $f(\text{RH}) = \sigma_{sp(\text{ambient})}/\sigma_{sp(\text{dry})}$, where $\sigma_{sp(\text{ambient})}$ and $\sigma_{sp(\text{dry})}$ are particle scattering coefficients at ambient and dry RH conditions, respectively) following the method developed by other investigators (Carrico et al., 1998; Kotchenruther and Hobbs, 1998; Carrico et al., 2000; Malm and Day, 2001; Sheridan et al., 2002; Magi and Hobbs, 2003; Kim et al., 2006). A difference between ambient and dry scattering coefficients is assumed to be caused solely by loss of water. Detailed derivations are provided in the Supplement. $f(\text{RH})$ is related to the particle scattering efficiencies (Q_s) and average particle diameter ($\overline{D_p}$) by

$$\overline{D_{p,\text{ambient}}} = \overline{D_{p,\text{dry}}} \sqrt{f(\text{RH}) \overline{Q_{s,\text{dry}}} / \overline{Q_{s,\text{ambient}}}} \quad (1)$$

$\overline{Q_{s,\text{ambient}}}$, $\overline{D_{p,\text{ambient}}}$ are the average scattering efficiency and average particle diameter under ambient conditions, while $\overline{Q_{s,\text{dry}}}$, $\overline{D_{p,\text{dry}}}$ represent dry conditions. The method is based on fine-particle light scattering being mostly due to particles in the accumulation mode and can be related to scattering efficiencies and the diameter of average surface, for both ambient and dry particle size distributions. Assuming that $\overline{Q_{s,\text{ambient}}} = \overline{Q_{s,\text{dry}}}$ (see Supplement Sect. 2 for justification and uncertainty analysis), it follows then that

$$\overline{D_{p,\text{ambient}}} = \overline{D_{p,\text{dry}}} \sqrt{f(\text{RH})} \quad (2)$$

Since the LWC is equal to the difference between ambient and dry particle volume, we get

$$f(\text{RH})_{\text{water}} = \left[f(\text{RH})^{1.5} - 1 \right] m_p \rho_w / \rho_p, \quad (3)$$

where m_p and ρ_p are dry particle mass and density, respectively; ρ_w is water density (constant 1 g cm⁻³ is applied). For SOAS, dry PM_{2.5} mass concentrations were measured continuously by a TEOM (tapered element oscillating microbalance, 1400a, Thermo Fisher Scientific Inc., operated by Atmospheric Research & Analysis Inc., referred to hereafter as ARA). Particle density, ρ_p , was computed from the particle composition, including AMS total organics, ammonium, and sulfate, which accounted for 90 % of the measured PM_{2.5} (TEOM) dry mass (SOAS study mean). A typical organic density 1.4 g cm⁻³ is assumed (Turpin and Lim, 2001; King et al., 2007; Engelhart et al., 2008; Kuwata et al., 2012; Cerully et al., 2014), and the density of ammonium sulfate is assumed to be 1.77 g cm⁻³ (Sloane et al., 1991; Stein et al., 1994). ρ_p was calculated to be 1.49 ± 0.04 g cm⁻³

Table 1. Deployment status of instruments at various sites. All the listed instruments or probes were operated at CTR for SOAS.

Site	Period	PILS-IC	AMS	CCNc	Nephelometer	TEOM	RH & T
JST	May & Nov 2012	No	Yes	No	No	Yes	Yes
YRK	Jul & Dec 2012	No	Yes	No	No	Yes	Yes
GIT	Jul–Aug 2012	No	Yes	No	No	Yes	Yes
RS	Sep 2012	No	Yes	No	No	Yes	Yes
CTR	Jun–Jul 2013	Yes	Yes	Yes	Yes	Yes	Yes

($n = 4393$) using mass fractions (ε):

$$\rho_p = \frac{1}{\varepsilon(\text{NH}_4^+ + \text{SO}_4^{2-})/1.77 + \varepsilon(\text{Organics})/1.4} \quad (4)$$

The time-resolved composition data show that dry-particle density did not have a significant diurnal variability ($\pm 2.7\%$, SD/mean, Supplement Fig. S2). In the following we refer to the particle water calculated by this method as $f(\text{RH})_{\text{water}}$. The uncertainty of $f(\text{RH})_{\text{water}}$ is estimated to be 15%, mainly caused by the calculation of $\overline{Q_{s,\text{ambient}}}/\overline{Q_{s,\text{dry}}}$ (LWC error of 10% from assuming $\overline{Q_{s,\text{ambient}}}/\overline{Q_{s,\text{dry}}} = 1$; see Supplement), m_p (10%), $\sigma_{\text{sp}(\text{ambient})}/\sigma_{\text{sp}(\text{dry})}$ (4.2%) (uncertainty for a single σ_{sp} measurement is 3%; Mitchell et al., 2009), and ρ_p (2.7%). Note that LWC error depends on RH, and for SOAS average aerosol composition could increase to 21% for RH > 90% (Supplement Fig. S6).

3 Modeling methods: predicting LWC and pH from aerosol composition

In most studies, such as SCAPE, particle water was not measured and must be determined based on aerosol composition. Both inorganic and organic components contribute to uptake of water vapor, establishing equilibrium for the ambient RH and T conditions. Thus, LWC is controlled by meteorological conditions and also by aerosol concentration and composition. Thermodynamic models, such as ISORROPIA-II, have been extensively used to predict LWC due to inorganic aerosol components (Fountoukis and Nenes, 2007). Contributions to LWC by organic components are typically based on an aerosol hygroscopicity parameter, κ , which is determined by CCN data. Here we refer to particle water associated with inorganics and organics as W_i and W_o , respectively. Total particle water ($W_i + W_o$) is taken as the sum of water associated with individual aerosol chemical components (sum of ions and lumped organics) based on the Zdanovskii–Stokes–Robinson (ZSR) relationship (Zdanovskii, 1936; Stokes and Robinson, 1966), with the assumption that the particles are internally mixed. The assumptions made in our analysis were discussed in Sect. 3.4.

3.1 LWC from inorganic species

Particle water associated with inorganic species (W_i) were predicted by ISORROPIA-II (Nenes et al., 1998; Fountoukis and Nenes, 2007). ISORROPIA-II calculates the composition and phase state of a $\text{K}^+ - \text{Ca}^{2+} - \text{Mg}^{2+} - \text{NH}_4^+ - \text{Na}^+ - \text{SO}_4^{2-} - \text{NO}_3^- - \text{Cl}^-$ -water inorganic aerosol in thermodynamic equilibrium with gas-phase precursors. Chemical and meteorological data are necessary inputs. For our analysis at CTR, the inputs to ISORROPIA-II are the inorganic ions measured by the IC or AMS, RH measured by the outside nephelometer, and temperature from the SEARCH site (ARA) meteorological data.

3.2 LWC from organic fraction

To determine the contributions to particle water by W_o , in SOAS the organic hygroscopicity parameter (κ_{org}) was calculated based on the observed CCN activities of the organic fraction (Cerully et al., 2014). In the following analysis diurnal 3 h running averages are used in the calculation. (Diurnal plot is included in the Supplement as Fig. S7). W_o is calculated using the following equation (Petters and Kreidenweis, 2007):

$$W_o = \frac{m_{\text{org}} \rho_w}{\rho_{\text{org}}} \frac{\kappa_{\text{org}}}{(1/\text{RH} - 1)}, \quad (5)$$

where m_{org} is the organic mass concentration from AMS (Xu et al., 2015), ρ_w is water density, and a typical organic density (ρ_{org}) of 1.4 g cm^{-3} is used (Turpin and Lim, 2001; King et al., 2007; Engelhart et al., 2008; Kuwata et al., 2012; Cerully et al., 2014).

3.3 pH prediction

The thermodynamic model ISORROPIA-II (Fountoukis and Nenes, 2007) calculates the equilibrium particle hydronium ion concentration per volume air (H_{air}^+), which along with the LWC is then used to predict particle pH. To correct for the LWC associated with the organic aerosol (not considered in ISORROPIA-II), we recalculate pH by considering H_{air}^+ and total predicted water (W_i and W_o).

The modeled concentrations are micrograms per cubic meter ($\mu\text{g m}^{-3}$) air for H_{air}^+ and LWC. The pH is, then,

$$\text{pH} = -\log_{10} \text{H}_{\text{aq}}^+ = -\log_{10} \frac{1000\text{H}_{\text{air}}^+}{W_i + W_o}, \quad (6)$$

where H_{aq}^+ (mol L^{-1}) is hydronium concentration in an aqueous solution. H_{air}^+ and W_i are the output of ISORROPIA-II based on input of water-soluble ions, RH, and T . H_{aq}^+ is H_{air}^+ divided by the LWC, and so including W_o decreases H_{aq}^+ by a factor of $W_o/(W_i + W_o)$, relative to only considering W_i .

ISORROPIA-II has been tested in previous field campaigns where a suite of both gas and particle components were measured (Nowak et al., 2006; Fountoukis et al., 2009). The model was able to predict the equilibrium partitioning of ammonia (Nowak et al., 2006) in Atlanta and nitric acid (Fountoukis et al., 2009) in Mexico City within measurement uncertainty. For instance, $\text{NH}_{3(\text{g})}$, NH_4^+ , $\text{HNO}_{3(\text{g})}$, and NO_3^- were within 10, 20, 80, and 20 % of measurements (Fountoukis et al., 2009). In this study, ISORROPIA-II was run in the “forward mode” for metastable aerosol. Forward mode calculates the equilibrium partitioning given the total concentration of various species (gas + particle) together with RH and T as input. Reverse mode involves predicting the thermodynamic composition based only on the aerosol composition. Here we use the forward mode with just aerosol-phase data input because it is less sensitive to measurement error than the reverse mode (Hennigan et al., 2015). The W_i prediction remains the same (reverse vs. forward: slope = 0.993, intercept = $-0.005 \mu\text{g m}^{-3}$, and $R^2 = 0.99$) no matter which approach is used. Gas-phase input does have an important impact on the H_{air}^+ calculation. ISORROPIA-II was tested with ammonia partitioning, which is discussed in more detail below. Here it is noted that we found that further constraining ISORROPIA-II with measured $\text{NH}_{3(\text{g})}$ (You et al., 2014) resulted in a pH increase of 0.8 at CTR and that the predicted $\text{NH}_{3(\text{g})}$ matched the measured $\text{NH}_{3(\text{g})}$ well (slope = 1.07, intercept = $-0.12 \mu\text{g m}^{-3}$, $R^2 = 0.76$). This also confirms that ISORROPIA-II predicts the pH in the ambient aerosol with reasonable accuracy, as inputting the total (gas + aerosol) ammonium results in predictions that agree with those observed. This is also in agreement with findings of Hennigan et al. (2015) and Fountoukis et al. (2009), both of whom found that ISORROPIA-II reproduced the partitioning of ammonia and inorganic nitrate in Mexico City during the Megacity Initiative: Local and Global Research Observations (MILARGO) campaign.

3.4 Assumptions

In the following analysis we use bulk properties and do not consider variability in parameters with particle size. Particulate organic and inorganic species are assumed to be internally mixed in the liquid phase due to the high RH ($74 \pm 16\%$) typical of this study and because a large frac-

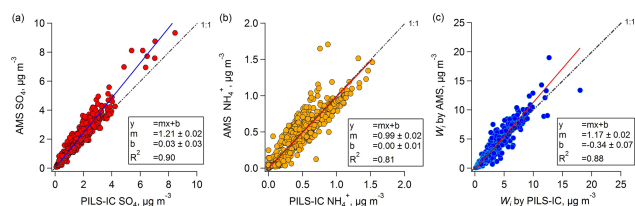


Figure 2. Comparisons of PM_{10} AMS sulfate, ammonium to PM_{10} and $\text{PM}_{2.5}$ PILS-IC (i.e., complete SOAS study) and predicted W_i . Orthogonal distance regression (ODR) fits were applied.

tion of the ambient aerosol organic component is from isoprene SOA (Xu et al., 2015), which are liquids at $\text{RH} \geq 60\%$ (Song et al., 2015). Particle liquid-phase separations are not considered, although they have been measured in bulk extracts of aerosols from the southeast (You et al., 2012). It is reported that liquid–liquid phase separation can occur when the O:C ratio of the organic material is ≤ 0.5 . More experiments showed that it is possible to have phase separation for $\text{O}:\text{C} \leq 0.7$, but not for $\text{O}:\text{C} \geq 0.8$ (Bertram et al., 2011; Song et al., 2012; You et al., 2013). SOAS average $\text{O}:\text{C} = 0.75 (\pm 0.12)$ is in the transition between these two regimes. According to Fig. 2 in Bertram et al. (2011), at RH typically $> 60\%$ and organic:sulfate mass ratio > 1 , it is not possible to have phase separation, which is the case for our sampling sites. Based on our basic assumption of no liquid–liquid phase separation, pH is considered to be homogeneous in a single particle. However, separated phases would likely have different pHs if liquid–liquid phase separation occurs. In that case, pH should be calculated based on the amounts of water and H_{air}^+ in each phase. Gas–particle phase partitioning will change accordingly, due to these separated phases. There are models that are set up to calculate these thermodynamics (e.g., AIOMFAC), but none is yet able to address the compositional complexity of ambient SOA (Zuend et al., 2010; Zuend and Seinfeld, 2012). Although it is often true that non-ideal interactions between organic and inorganic species exist, good agreement between measured particle water and ammonia partitioning to predictions using the bulk properties (discussed below) suggests these assumptions are reasonable.

4 Results

4.1 Overall summary of meteorology and PM composition at SOAS and SCAPE sites

For the SOAS study period, mean T and RH were $25 \pm 3^\circ$ and $74 \pm 16\%$ (mean \pm SD), respectively. This resulted in a $f(\text{RH})_{\text{water}}$ level of $4.5 \pm 3.8 \mu\text{g m}^{-3}$, with a maximum value of $28.4 \mu\text{g m}^{-3}$. In comparison, SOAS mean dry $\text{PM}_{2.5}$ mass was $7.7 \pm 4.6 \mu\text{g m}^{-3}$, implying that the fine aerosols were roughly composed of 37 % water, on average. Mean T and RH for SCAPE sites are listed in Table 3. Summer T

means were all above 21°, including CTR. RH means were all high (> 60 %) for summer and winter, which is typical for the southeastern US.

Of the sites in the southeastern US discussed in this paper, CTR was the least influenced by anthropogenic emissions having the lowest black carbon (BC) concentrations (measured by a MAAP, Thermo Scientific, model 5012). At CTR, the mean BC = $0.3 \pm 0.2 \mu\text{g m}^{-3}$ (\pm SD), whereas mean BC concentrations at the other rural site (YRK) was $0.4 \mu\text{g m}^{-3}$. The representative Atlanta site (JST) BC was on average $0.7 \mu\text{g m}^{-3}$, and higher for sites closer to roadways: $1.0 \mu\text{g m}^{-3}$ (GIT) and $2.0 \mu\text{g m}^{-3}$ (RS).

A more comprehensive suite of ions will provide a better prediction of W_i . However, in the southeastern USA, inorganic ions are currently dominated by sulfate and ammonium. During SOAS, the PILS-IC provided a more comprehensive and accurate measurement of water-soluble ions than AMS, which measured only non-refractory sulfate, ammonium, nitrate, and chloride. Refractory but water-soluble ions, such as sodium and associated chloride, and crustal elements including calcium, potassium, and magnesium were present in PM_{10} , but in very low concentrations. Contributions of these ions are more important in $\text{PM}_{2.5}$ than for PM_{10} , which tend to reduce aerosol acidity. For instance, Na^+ has a significantly higher mean in $\text{PM}_{2.5}$ at $0.056 \mu\text{g m}^{-3}$ (first half of SOAS study) than $0.001 \mu\text{g m}^{-3}$ in PM_{10} (second half of SOAS study). Four 1-day-long dust events (12, 13, 16, and 21 June) in the SOAS data set have been excluded from this analysis as assumptions relating to internal mixing of $\text{PM}_{2.5}$ components are less valid in these cases. Excluding these days, the mean Na^+ in $\text{PM}_{2.5}$ drops to $0.024 \mu\text{g m}^{-3}$.

If the fraction of the refractory ions (e.g., Na^+ , K^+ , Ca^{2+} , Mg^{2+}) is negligible compared to the SO_4 (note that SO_4 stands for sulfate in all its possible forms, from free to completely dissociated), NH_4^+ , and NO_3^- , the AMS data sufficiently constrain particle composition for thermodynamic calculations; this apparently is the case for most of the time in the southeast (Supplement Sect. 4). For PM_{10} SO_4 and NH_4^+ , AMS and PILS-IC were in good agreement (SO_4 slopes within 20 %, $R^2 = 0.90$; NH_4^+ within 1 %, $R^2 = 0.81$). Similar agreement was also found for AMS PM_{10} SO_4 and NH_4^+ versus PILS-IC $\text{PM}_{2.5}$ SO_4 and NH_4^+ (see Fig. 2 for comparison of complete data set). These data indicate little SO_4 and NH_4^+ between the 1.0 and $2.5 \mu\text{m}$ size range ($\text{PM}_{2.5}$ – PM_{10}). Because of the agreement between these dominant ions, ISORROPIA-II predicted W_i for all ions measured with the PILS-IC throughout the study (includes both PM_{10} and $\text{PM}_{2.5}$) agreed with W_i based on AMS inorganic species (i.e., only ammonium and sulfate) having an orthogonal slope of 1.18 (Fig. 2c).

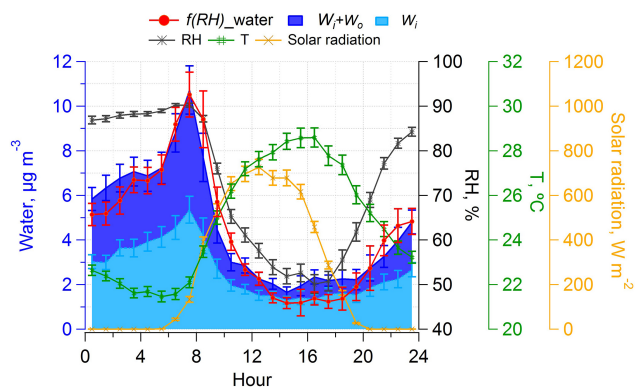


Figure 3. CTR (SOAS) diurnal profiles of predicted and measured water, measured RH, T , and solar radiation. Median hourly averages are shown, and standard errors are plotted as error bars.

4.2 Results from the SOAS Centreville site

4.2.1 LWC, pH, and ion balances at Centreville

The diurnal variation of LWC contributed by W_i and W_o , along with total measured water, ambient T , RH, and solar radiation at CTR is shown in Fig. 3. Predicted and measured LWC trends were in good overall agreement, although the largest discrepancy was observed during the daytime, when the LWC level was low and more difficult to measure and accurately predict. Nighttime RH median values were between 85 and 90 % and resulted in significant water uptake that reached a peak just after sunrise near 07:30 (local time). The dramatic peak in LWC starting at roughly 05:00 and reaching a maximum between 07:30 and 08:00 is likely due to RH increasing above 90 %, at which point uptake of water rapidly increases with increasing RH. The similar rapid hygroscopic growth before sunrise was also observed here at GIT, RS, and JST (November) (Fig. 11). After sunrise, rising temperatures led to a rapid drop in RH, resulting in rapid loss of particle water. LWC reached lowest levels ($\sim 2 \mu\text{g m}^{-3}$) in the afternoon, only 20 % of the peak value. W_o varied more than W_i diurnally; W_o max / min ratio was 13.1, compared to 4.1 for W_i .

At CTR, the aerosol was highly acidic, with predicted mean pH = 0.94 ± 0.59 (\pm SD). The minimum and maximum pH were -0.94 and 2.23 , respectively, and pH varied by approximately 1 on average throughout the day (Fig. 4a); that is, the $\text{H}_{\text{air}}^+ / \text{LWC}$ ratio increased by a factor of 10 from night to day. LWC max / min ratio was 5, whereas H_{air}^+ diurnal variation was significantly less (Fig. 4b), indicating that the diurnal pattern in pH was mainly driven by particle water dilution. This is further demonstrated in Fig. 4d, which shows the diurnal variation in the $\text{NH}_4^+ / \text{SO}_4^{2-}$ molar ratio (the main ions driving pH), with only slightly lower ratios during the day. The study mean (\pm SD) $\text{NH}_4^+ / \text{SO}_4^{2-}$ molar ratio was $1.4 (\pm 0.5)$. As LWC is mainly controlled by RH and tem-

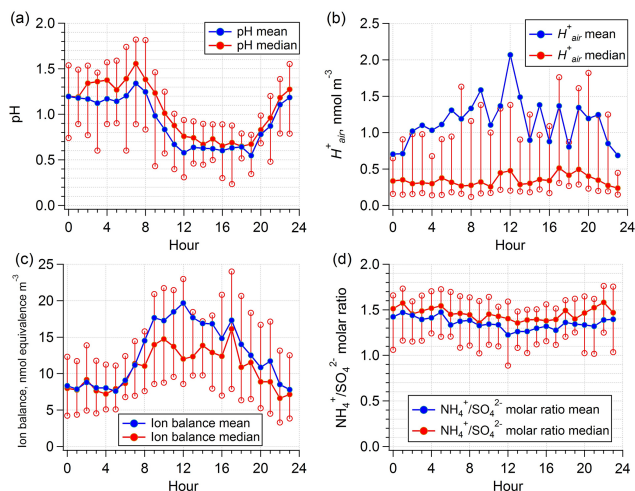


Figure 4. CTR (SOAS) diurnal patterns of calculated pH based on total predicted water ($W_i + W_o$) (a), H_{air}^+ predicted by ISORROPIA-II (b), ion balance (c), and $\text{NH}_4^+/\text{SO}_4^{2-}$ molar ratio (d). Mean and median values are shown, together with 25 and 75 % quantiles marked as non-filled circles.

perature, the pH diurnal variation was thus largely driven by meteorological conditions, not aerosol composition.

In part because of the diurnal variation of LWC, a simple ion balance or $\text{NH}_4^+/\text{SO}_4^{2-}$ molar ratio or per-volume-air concentration of aerosol hydronium ion (H_{air}^+) alone cannot be used as a proxy for pH in the particle. Figure 5a shows a weak inverse correlation ($R^2 = 0.36$) between ion balance and pH. An ion balance of an aerosol is usually calculated as follows (in units of nmol equivalence m^{-3}) for a $\text{NH}_4^+ - \text{Na}^+ - \text{SO}_4^{2-} - \text{NO}_3^- - \text{Cl}^-$ - water inorganic aerosol:

$$\text{ion balance} = \frac{[\text{SO}_4^{2-}]}{48} + \frac{[\text{NO}_3^-]}{62} + \frac{[\text{Cl}^-]}{35.5} - \frac{[\text{NH}_4^+]}{18} - \frac{[\text{Na}^+]}{23}, \quad (7)$$

where $[\text{SO}_4^{2-}]$, $[\text{NO}_3^-]$, $[\text{Cl}^-]$, $[\text{NH}_4^+]$, and $[\text{Na}^+]$ are concentrations of these ions in units of grams per cubic meter (g m^{-3}). An ion balance is also a bad indicator of pH because it poorly predicts the aerosol concentration of H_{air}^+ . An ion balance assumes all ions are completely dissociated, but multiple forms are possible, depending on pH (e.g., sulfate can be in the form of H_2SO_4 , HSO_4^- , or SO_4^{2-}). For example, if aerosol sulfate remains in the free form of H_2SO_4 , it does not add protons. Thus, an ion balance usually overestimates protons and is only moderately correlated with H_{air}^+ (Fig. 5b).

4.2.2 LWC uncertainty

In estimating the water uncertainty, we consider W_i and W_o separately. The uncertainty of W_i is estimated by propagat-

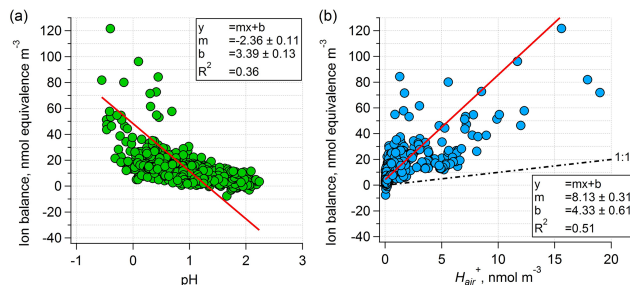


Figure 5. Comparison of ion balance to pH (a) and to H_{air}^+ (b) at CTR (SOAS). An ODR fit was applied.

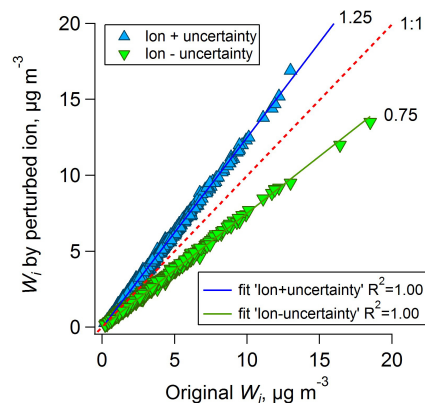


Figure 6. W_i based on artificially perturbed ion data at upper and lower uncertainty limits is compared to W_i at base level. The slopes indicate the W_i uncertainty caused by ions.

ing the measurement uncertainty of ions and RH through the ISORROPIA-II thermodynamic model by finite perturbations about the model base state. Uncertainties of ions were estimated by difference between IC ions and AMS ions, as well as PILS-IC measurement uncertainty (Table 2). Na^+ is excluded because it is not measured by the AMS. PILS-IC instrumental uncertainty is estimated to be 15 % from the variability in standards (variability is calibration slopes), blanks, sample airflow rate, and liquid flow rate (one SD). The total ion uncertainties are listed in Table 2. SO_4 has a higher uncertainty, at 25 %, than the rest, which are at 15 %. These combined uncertainties lead to an W_i uncertainty of 25 % (Fig. 6), which is the same as the SO_4 uncertainty. SO_4 , one of the most hygroscopic ions (Petters and Kreidenweis, 2007), controls W_i uptake.

For the SOAS study, the RH probe in the ambient nephelometer (Humitter 50U, VAISALA Inc.) has a stated maximum uncertainty of 5 % at $\text{RH} = 90 \%$. RH biases with respect to environment conditions can also occur due to placement of the probe. Based on RH comparisons between ARA, Rutgers (Nguyen et al., 2014), and the Georgia Tech instrumentation, a systematic bias as large as 10 % is found. Given this, we consider an RH probe factory uncertainty (5 %) as a typical value and intercomparison difference (10 %) as an

Table 2. Sensitivity of H_{air}^+ to ions from ANISORROPIA (second row) and contribution to uncertainty. Uncertainties of inorganic ions ($\frac{\delta_{\text{Ion}}}{\text{Ion}}$) are calculated based on a combination of PILS-IC instrumental relative uncertainties (IC uncertainty, referred to as $\frac{\delta_{\text{Ion,IC}}}{\text{Ion}}$, all estimated to be 15 %) and the difference between PILS-IC and AMS ($\frac{\delta_{\text{Ion,IC-AMS}}}{\text{Ion}}$, defined as the (slope – 1) in Fig. 2a and 2b) (third row), where $\frac{\delta_{\text{Ion}}}{\text{Ion}} = \sqrt{\left(\frac{\delta_{\text{Ion,IC}}}{\text{Ion}}\right)^2 + \left(\frac{\delta_{\text{Ion,IC-AMS}}}{\text{Ion}}\right)^2}$ (fourth row). Contribution of uncertainty is the ratio of ion uncertainty over H_{air}^+ uncertainty ($\frac{\delta_{H_{\text{air}}^+}}{H_{\text{air}}^+}$, calculated to be 14 % in Eq. 8) (fifth row).

PILS-IC ion concentration, $\mu\text{g m}^{-3}$ (mean \pm SD)	SO_4	NH_4^+	Na^+	NO_3^-	Cl^-
	1.73 ± 1.21	0.46 ± 0.34	0.03 ± 0.07	0.08 ± 0.08	0.02 ± 0.03
H_{air}^+ Sensitivity (mean \pm SD)	$\left \frac{\partial H_{\text{air}}^+}{\partial \text{SO}_4}\right $	$\left \frac{\partial H_{\text{air}}^+}{\partial \text{NH}_4^+}\right $	$\left \frac{\partial H_{\text{air}}^+}{\partial \text{Na}^+}\right $	$\left \frac{\partial H_{\text{air}}^+}{\partial \text{NO}_3^-}\right $	$\left \frac{\partial H_{\text{air}}^+}{\partial \text{Cl}^-}\right $
	0.51 ± 0.34	0.32 ± 0.31	0.19 ± 0.27	0.002 ± 0.007	0.000 ± 0
$\frac{\delta_{\text{Ion,IC-AMS}}}{\text{Ion}}$	$\frac{\delta_{\text{SO}_4,\text{IC-AMS}}}{\text{SO}_4}$	$\frac{\delta_{\text{NH}_4^+,\text{IC-AMS}}}{\text{NH}_4^+}$	$\frac{\delta_{\text{Na}^+,\text{IC-AMS}}}{\text{Na}^+}$	$\frac{\delta_{\text{NO}_3^-\text{,IC-AMS}}}{\text{NO}_3^-}$	$\frac{\delta_{\text{Cl}^-\text{,IC-AMS}}}{\text{Cl}^-}$
	20.5 %	1.5 %	N/A ^a	b	b
$\frac{\delta_{\text{Ion}}}{\text{Ion}}$	$\frac{\delta_{\text{SO}_4}}{\text{SO}_4}$	$\frac{\delta_{\text{NH}_4^+}}{\text{NH}_4^+}$	$\frac{\delta_{\text{Na}^+}}{\text{Na}^+}$	$\frac{\delta_{\text{NO}_3^-}}{\text{NO}_3^-}$	$\frac{\delta_{\text{Cl}^-}}{\text{Cl}^-}$
	25.4 %	15.1 %	15 %	15 %	15 %
Contribution to H_{air}^+ uncertainty	$\frac{\left \frac{\partial H_{\text{air}}^+}{\partial \text{SO}_4}\right \cdot \frac{\delta_{\text{SO}_4}}{\text{SO}_4}}{\frac{\delta_{H_{\text{air}}^+}}{H_{\text{air}}^+}}$	$\frac{\left \frac{\partial H_{\text{air}}^+}{\partial \text{NH}_4^+}\right \cdot \frac{\delta_{\text{NH}_4^+}}{\text{NH}_4^+}}{\frac{\delta_{H_{\text{air}}^+}}{H_{\text{air}}^+}}$	$\frac{\left \frac{\partial H_{\text{air}}^+}{\partial \text{Na}^+}\right \cdot \frac{\delta_{\text{Na}^+}}{\text{Na}^+}}{\frac{\delta_{H_{\text{air}}^+}}{H_{\text{air}}^+}}$	$\frac{\left \frac{\partial H_{\text{air}}^+}{\partial \text{NO}_3^-}\right \cdot \frac{\delta_{\text{NO}_3^-}}{\text{NO}_3^-}}{\frac{\delta_{H_{\text{air}}^+}}{H_{\text{air}}^+}}$	$\frac{\left \frac{\partial H_{\text{air}}^+}{\partial \text{Cl}^-}\right \cdot \frac{\delta_{\text{Cl}^-}}{\text{Cl}^-}}{\frac{\delta_{H_{\text{air}}^+}}{H_{\text{air}}^+}}$
	0.93	0.35	0.20	0.002	0.000

^a Na^+ is not measured by AMS. ^b $\left|\frac{\partial H_{\text{air}}^+}{\partial \text{NO}_3^-}\right|$ and $\left|\frac{\partial H_{\text{air}}^+}{\partial \text{Cl}^-}\right|$ are less than 1 % of the other H_{air}^+ sensitivities, and the loadings of NO_3^- and Cl^- are less than 5 % of the total inorganic ion mass. As a result, their contributions to H_{air}^+ uncertainty are negligible.

extreme condition. In this analysis, RH was adjusted by ± 5 and ± 10 %, and W_i recalculated (Fig. 7). A ± 5 % perturbation in RH leads to a 91 % (slope – 1) error for 5 % perturbation above the measured value (1.05 RH) and 29 % error for a perturbation below the measured value (0.95 RH). We take 60 % as average uncertainty. Higher uncertainty is introduced with increasing RH, owing to the exponential growth of LWC with RH, and results in the asymmetric LWC uncertainty. Combining W_i uncertainty from ions (25 %) and RH (60 %), the overall uncertainty is calculated as 65 %.

The uncertainty sources for W_o are κ_{org} , ρ_s , m_s , and RH (Eq. 5). The uncertainties of these parameters are estimated to be 26 (details can be found in Supplement Sect. 3), 10, 20, and 5 % (from above), respectively. In summary, the overall uncertainty of W_o is 35 %.

The total uncertainty of LWC can be expressed as a sum of W_i and W_o uncertainties, where ε_i is the mass fraction. ε_{W_o} was found to be 36 %, and ε_{W_i} was 64 %.

$$\frac{\delta_{\text{LWC}}}{\text{LWC}} = \sqrt{\left(\varepsilon_{W_i} \frac{\delta_{W_i}}{W_i}\right)^2 + \left(\varepsilon_{W_o} \frac{\delta_{W_o}}{W_o}\right)^2} \quad (8)$$

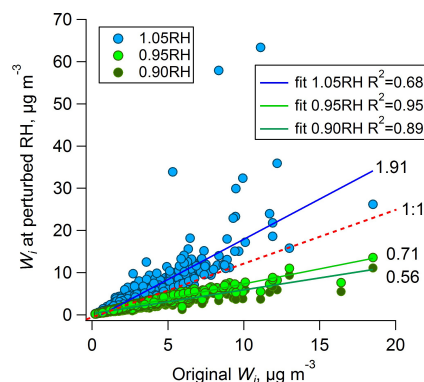


Figure 7. W_i based on artificially perturbed RH at upper and lower uncertainty limits compared to W_i at base level. 1.10 RH (i.e., RH increased by 10 %) is not plotted because it results in much larger W_i than the rest. Slopes and R^2 indicate corresponding W_i uncertainty caused by variability (uncertainty) in RH.

Given the above, $\frac{\delta_{\text{LWC}}}{\text{LWC}}$ is 43 %. This method of assessing predicted LWC uncertainty can be applied to SCAPE sites as well. The specific predicted LWC at SCAPE sites was calculated and is listed in Table 3. W_i uncertainty associated with

Table 3. Water and pH prediction for SCAPE sites. Means and SDs are listed, if not specified. Total ion concentration is counted as the sum of AMS inorganics (third row). ε_{W_o} is the mass fraction of W_o (fifth row).

	JST May 2012	YRK Jul 2012	GIT Aug 2012	RS Sep 2012	JST Nov 2012	YRK Dec 2012
RH, %	67 ± 19	66 ± 21	71 ± 17	72 ± 20	63 ± 19	73 ± 21
T , °	23 ± 4	28 ± 4	26 ± 4	21 ± 4	12 ± 5	10 ± 5
Total ion concentration, $\mu\text{g m}^{-3}$	4.1 ± 2.1	4.5 ± 2.2	5.3 ± 2.6	4.1 ± 2.7	3.6 ± 2.1	2.3 ± 1.8
$\frac{\delta_{\text{pH}}}{\text{pH}}$ from 1.10 RH	22.3%	21.4%	48.3%	22.1%	2.5%	1.4%
Total $\frac{\delta_{\text{pH}}}{\text{pH}}$	23.9%	23.0%	49.0%	23.7%	8.8%	8.6%
ε_{W_o} , %	34 ± 11	37 ± 8	33 ± 10	38 ± 11	39 ± 16	29 ± 15
LWC, $\mu\text{g m}^{-3}$	6.0 ± 6.3	8.1 ± 8.5	8.4 ± 7.7	7.8 ± 9.2	5.9 ± 8.7	3.2 ± 3.5
pH*	1.3 ± 0.7	1.1 ± 0.6	1.1 ± 0.4	1.3 ± 0.7	2.2 ± 0.9	1.8 ± 1.0
LWC, $\mu\text{g m}^{-3}$ (median)	3.7 ± 6.3	5.3 ± 8.5	6.1 ± 7.7	4.3 ± 9.2	2.1 ± 8.7	2.0 ± 3.5
pH* (median)	1.2 ± 0.7	1.0 ± 0.6	1.0 ± 0.4	1.2 ± 0.7	2.3 ± 0.9	1.8 ± 1.0

* A bias correction of 1 pH unit is applied due to not considering ammonia partitioning. See Sect. 4.2.5 for details.

ions is the same as noted above, 25 %, because it is estimated by PILS-IC and AMS differences. Similar uncertainties in W_i at the SCAPE sites are expected if RH uncertainties are similar at all sites.

4.2.3 pH uncertainty

As pH is based on H_{air}^+ and LWC, the uncertainty of pH can be estimated from these two parameters. We applied the adjoint model of ISORROPIA, ANISORROPIA (Capps et al., 2012), to quantify the sensitivity of predicted H_{air}^+ to the input aerosol species at the conditions of the thermodynamic calculations. pH uncertainty resulting from aerosol composition is then determined by propagating the input parameter uncertainties, using ANISORROPIA sensitivities, to the corresponding H_{air}^+ and pH uncertainty.

We now assess how pH of $\text{PM}_{2.5}$ is affected by using an incomplete measurement of ionic species by comparing the pH predicted based on the more complete suite of ions measured by the PILS-IC versus the AMS, during SOAS. Sensitivities of aerosol species to H_{air}^+ were calculated by ANISORROPIA with PILS-IC data and presented as partial derivatives (Table 2). Higher sensitivity values imply the inorganic ion is more important for H_{air}^+ . In the SOAS study, H_{air}^+ is most sensitive to SO_4 , and then NH_4^+ , as they were the major ions. Uncertainties of ions were estimated by the difference between IC ions and AMS ions, as well as PILS-IC measurement uncertainty. Since Na^+ is not measured by AMS, we cannot estimate the difference between PILS-IC and AMS. The loadings and sensitivities of NO_3^- and Cl^- were very low, so they

are assumed not to contribute much to $\frac{\delta_{H_{\text{air}}^+}}{H_{\text{air}}^+}$. Given this, $\frac{\delta_{H_{\text{air}}^+}}{H_{\text{air}}^+}$ is determined by

$$\frac{\delta_{H_{\text{air}}^+}}{H_{\text{air}}^+} = \sqrt{\left(\frac{\partial H_{\text{air}}^+}{\partial \text{SO}_4} \frac{\delta_{\text{SO}_4}}{\text{SO}_4}\right)^2 + \left(\frac{\partial H_{\text{air}}^+}{\partial \text{NH}_4^+} \frac{\delta_{\text{NH}_4^+}}{\text{NH}_4^+}\right)^2 + \left(\frac{\partial H_{\text{air}}^+}{\partial \text{Na}^+} \frac{\delta_{\text{Na}^+}}{\text{Na}^+}\right)^2} \quad (9)$$

Based on the input for Eq. (9) (Table 2), $\frac{\delta_{H_{\text{air}}^+}}{H_{\text{air}}^+}$ is estimated as 14 %. LWC is most sensitive to RH fluctuations, so it is considered the main driver of LWC uncertainty in the pH calculation. As discussed, we artificially adjusted RH by ± 5 and ± 10 % (10 % is considered an extreme condition). H_{air}^+ , W_i , W_o , and pH were all recalculated using 90, 95, 105, and 110 % of the actual measured RH. RH + 5 % and RH – 5 % lead to 12 and 6 % variation in pH based on orthogonal regression slopes, respectively (Fig. 8). RH – 10 % results in only 10 % variation; however, RH + 10 % results in a 45 % variation, and the coefficient of determination (R^2) between pH calculated based on RH + 10 % and original RH drops to only 0.78, while for all other cases $R^2 > 0.96$. The disproportionately large effect of the positive uncertainty is caused by the exponential increase of LWC with RH, as RH reaches high levels (> 90 %). Assuming the stated manufacturer uncertainty (5 %) for our RH uncertainty, pH uncertainty is estimated to be 6–12 %. We take 12 % as $\frac{\partial \text{pH}}{\partial \text{LWC}} \delta_{\text{LWC}}$ for further calculations.

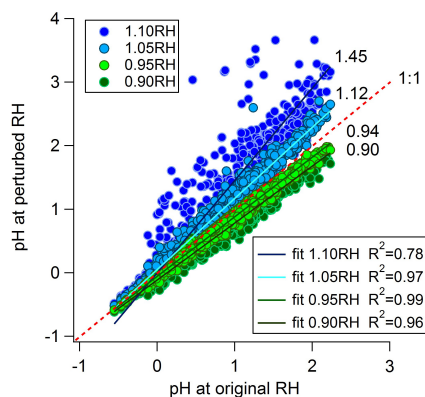


Figure 8. pH predictions by perturbing RH compared to pH at base level. W_i , W_o , and H_{air}^+ were recalculated based on ± 5 and $\pm 10\%$ original RH to investigate pH uncertainty. The slopes and R^2 indicate pH uncertainty caused by RH.

SO_4 was found to contribute the most to $\frac{\delta H_{\text{air}}^+}{H_{\text{air}}^+}$. NH_4^+ and Na^+ followed. SO_4 and NH_4^+ are the two most abundant inorganic components in aerosols and controlling aerosol acidity. Finally, the total pH uncertainty is the combination of LWC and the uncertainty associated with H_{air}^+ , which is computed from the definition of pH (Eq. 6).

$$\frac{\delta_{\text{pH}}}{\text{pH}} = \sqrt{\left(\frac{\partial \text{pH}}{\partial H_{\text{air}}^+} \delta_{H_{\text{air}}^+}\right)^2 + \left(\frac{\partial \text{pH}}{\partial \text{LWC}} \delta_{\text{LWC}}\right)^2}, \quad (10)$$

where $\frac{\partial \text{pH}}{\partial H_{\text{air}}^+}$ can be derived from Eq. (6) as

$$\frac{\partial \text{pH}}{\partial H_{\text{air}}^+} = -\frac{1}{2.303} \frac{1}{\frac{H_{\text{air}}^+}{\text{LWC}}} \frac{1}{\text{LWC}} = -\frac{1}{2.303} \frac{1}{H_{\text{air}}^+}. \quad (11)$$

From Eq. (9) and the uncertainties of H_{air}^+ and LWC (Eqs. 7 and 8), we estimate the pH uncertainty for the SOAS data set to be 13% (based on the specific uncertainties considered here). pH uncertainties at SCAPE sites were also assessed via this method. As discussed above, $\frac{\delta H_{\text{air}}^+}{H_{\text{air}}^+}$ was found to be 14% for the SOAS study, due to IC and AMS data set differences and PILS-IC instrumental uncertainty. This same uncertainty is applied to SCAPE, where no PILS-IC data were available. Because aerosol composition at all sites is similar, based on filter IC analysis (Supplement Fig. S8), similar sensitivities of H_{air}^+ to ions are expected. However, actual uncertainty for each sampling period is possibly higher due to higher loadings of refractory ions at SCAPE sites due to contributions from urban emissions. Refractory ions not measured by the AMS (i.e., Na^+ , K^+ , Ca^{2+} , Mg^{2+}) have a minor effect on predicting LWC but may have an important effect on pH (e.g., result in higher pH) in locations where they could substantially contribute to the overall ion balance.

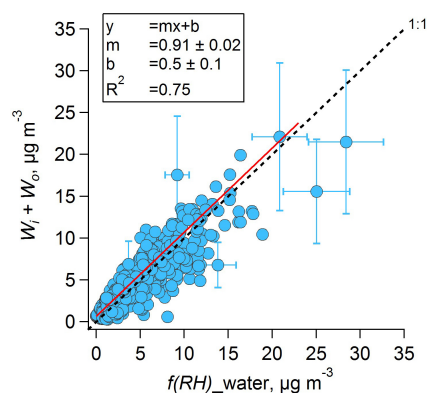


Figure 9. Comparison between total predicted and measured water by nephelometers based on hourly averaged data at CTR (SOAS). An ODR fit was applied. Error bars for selected points are shown.

4.2.4 Model validation: prediction of liquid water

Several LWC measurements were made at CTR during SOAS. In addition to $f(\text{RH})_{\text{water}}$ ($4.5 \pm 3.8 \mu\text{g m}^{-3}$), particle water was quantified with a semi-volatile differential mobility analyzer (SVDMA). With this method, a SOAS study mean particle water concentration of $4.3 \pm 3.7 \mu\text{g m}^{-3}$ ($\pm \text{SD}$) was obtained (Nguyen et al., 2014). The orthogonal regression between these two measurements (SVDMA water vs. $f(\text{RH})_{\text{water}}$) has slope = 0.91, intercept = $-0.0 \mu\text{g m}^{-3}$, and $R^2 = 0.35$. Differences could be caused by differences in size-resolved composition (particle composition beyond PM_{10} that contributes LWC; SVDMA scans up to $1.1 \mu\text{m}$, while $f(\text{RH})_{\text{water}}$ is based on $\text{PM}_{2.5}$), instrument sample heating (i.e., the degree to which the instrument was close to ambient conditions, especially when ambient RH was high, and most sensitive to slight T differences), and differences in RH probe calibrations.

CTR-predicted total LWC ($W_i + W_o$) was $5.1 \pm 3.8 \mu\text{g m}^{-3}$ and agreed well with $f(\text{RH})_{\text{water}}$. The total predicted water was highly correlated and on average within 10% of the measured water, with slope = 0.91, intercept = $0.5 \mu\text{g m}^{-3}$, and $R^2 = 0.75$ (see Fig. 9). Since excluding refractory ions (Sect. 4.1) and not considering gas-phase species in the ISORROPIA-II calculations do not significantly affect the LWC prediction, its comparison across sites is less uncertain than pH.

4.2.5 Model validation: prediction of pH

ISORROPIA-II calculations of pH at CTR for the SOAS study were evaluated by comparing measured and predicted $\text{NH}_3(\text{g})$. Although NH_4^+ and $\text{NH}_3(\text{g})$, along with other aerosol components, are input into the model, comparing ambient NH_4^+ and $\text{NH}_3(\text{g})$ to model predictions is not a circular analysis. For each observed data point, the model calculates total ammonia from the NH_4^+ and $\text{NH}_3(\text{g})$ input, and then calcu-

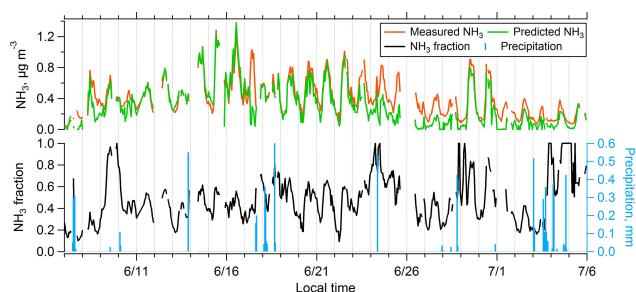


Figure 10. CTR (SOAS) time series of hourly averaged measured $\text{NH}_3(\text{g})$, predicted $\text{NH}_3(\text{g})$, $\text{NH}_3(\text{g})$ fraction (i.e., measured $\text{NH}_3(\text{g}) / (\text{NH}_3(\text{g}) + \text{NH}_4^+)$), and precipitation.

lates the gas–particle ammonia partitioning assuming equilibrium. There are also other various assumptions/limitations associated with the model. Figure 10 shows the SOAS study time series of measured and predicted $\text{NH}_3(\text{g})$ and the fraction of ammonia in the gas phase ($\text{NH}_3(\text{g}) / (\text{NH}_3(\text{g}) + \text{NH}_4^+)$). Measured and predicted $\text{NH}_3(\text{g})$ are in good agreement. Periods when almost all ammonia was in the gas phase (ratio near 1) are related to precipitation events (10, 24, 28 June; 3, 4 July) when aerosol concentrations were very low. Not including these events, the study mean ($\pm\text{SD}$) fraction ammonia in the gas phase was 0.41 (± 0.16) (median value is also 0.41). These results provide confidence in ISORROPIA-II calculations of particle pH and demonstrate the utility of including both measurements of particle and gas phases in these types of studies.

When gas data are not available, pH predictions are not as accurate (Hennigan et al., 2015). Running ISORROPIA-II in the forward mode, but with only aerosol concentrations as input, may result in a bias in predicted pH due to repartitioning of ammonia in the model. In the southeast, where pH is largely driven by SO_4 and NH_4^+ , the aerosol NH_4^+ input will be partitioned in the model between gas and particle phases to establish equilibrium. Sulfate repartitioning does not occur since it is non-volatile. Thus, NH_4^+ will be lost from the particle and a lower pH predicted. At CTR ammonia partitioning has been included in all model runs, but no $\text{NH}_3(\text{g})$ was available for SCAPE. Assuming the average $\text{NH}_3(\text{g}) / \text{NH}_4^+$ ratio from CTR applies to all SCAPE sites to estimate $\text{NH}_3(\text{g})$, along with measured particle composition at each site, we got pH increases ranging from 0.87 to 1.38. In the following, all pHs reported for SCAPE are corrected for this bias (i.e., pHs are increased by 1 to simplify the correction). Note that ammonia partitioning does not significantly affect the LWC prediction (W_i predicted without $\text{NH}_3(\text{g})$ vs. W_i predicted with $\text{NH}_3(\text{g})$: slope = 1.00, intercept = $-0.01 \mu\text{g m}^{-3}$, $R^2 = 0.98$).

4.3 LWC and pH at other sites in the southeast (SCAPE sites)

4.3.1 Seasonal trends

The methods developed and verified at CTR are now applied to the SCAPE study, where fewer species were measured. LWC predictions at all SCAPE sites are shown in Table 3, providing insights on seasonal trends of LWC in the southeast. The overall summer LWC mean was $5.0 \mu\text{g m}^{-3}$ and winter mean $2.2 \mu\text{g m}^{-3}$.

At the SCAPE sites – JST, YRK, GIT, and RS – summer mean pHs were between 1 and 1.3, similar to CTR (mean of 0.94). In winter the pHs (mean between 1.8 and 2.2) were higher by ~ 1 unit. Although LWC was higher in summer, which tends to dilute H_{air}^+ and increase pH, summer pH was lower due to higher ion (i.e., sulfate) concentrations (Table 3). Similar diurnal pH patterns were seen at all sites in all seasons and follow the diurnal variations of particle water (Fig. 11). Overall the pH in the southeast is very low, between 1 and 2 (mean), in both rural and urban environments. pH values in summer at various sites were similar (1 to 1.3), suggesting a fairly homogeneous distribution of acidity due to spatially uniform sulfate in the southeastern US (Zhang et al., 2012). In winter the diurnal range in pH was roughly 2 units, while the diurnal range in summer was smaller, with pH varying by roughly 1.

Recall that, at CTR, 10% RH uncertainty can result in a pH prediction error of up to 45% due to the high RHs observed during the study. We estimated pH uncertainty from W_i and W_o by +10% RH for each SCAPE site. As Table 3 shows, the pH uncertainty associated with RH is much lower in winter (only 1–3%) than summer (20–40%), although RH averages were similar, e.g., JST in May ($67 \pm 19\%$) and November ($63 \pm 19\%$), with even higher RH in winter at YRK. Total pH uncertainty at all SCAPE sites is calculated by the same method as CTR. Table 3 shows that higher RH and T result in larger pH uncertainty. In summer, pH uncertainty is mainly caused by RH, while in winter it can be attributed mostly to uncertainty in ion concentrations.

4.3.2 The role of W_o

W_o was significant, accounting for on average 29–39% of the total $\text{PM}_{2.5}$ particle water for all our sites (Fig. 12 and Table 3). Note that W_o at SCAPE sites was calculated by in situ AMS measurements at each SCAPE site and the mean κ_{org} (0.126) measured at CTR, due to lack of CCNc. Note that ε_{W_o} could be higher or lower at each site depending on the type of organics presented and the related κ_{org} . Figure 12 shows that W_o is related to the organic mass fraction. W_o is comparable to W_i at night. In contrast, it was only 33% of W_i during the daytime (Fig. 3). The significant fraction, even during daytime, indicates organic aerosol components will have a considerable contribution to aerosol radiative forcing.

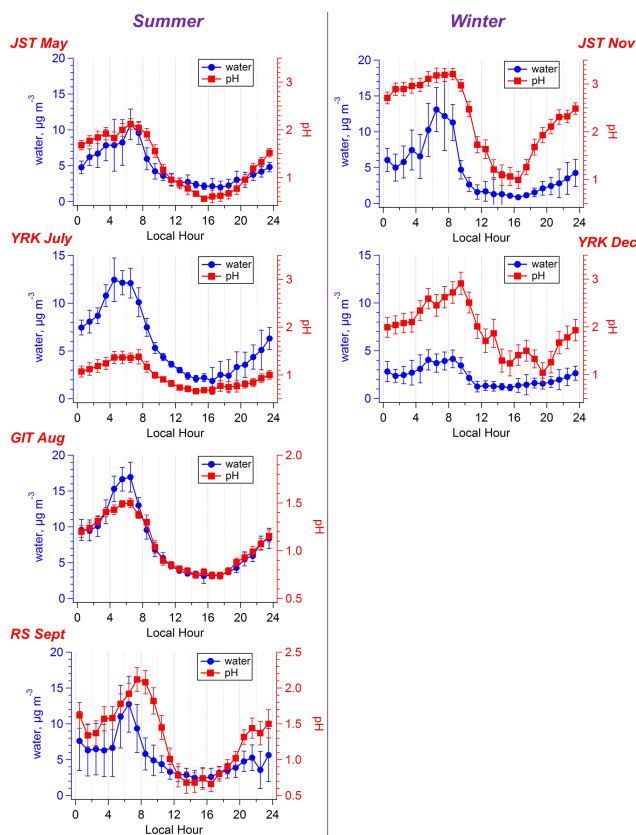


Figure 11. LWC and pH diurnal variation at SCAPE sites: comparison between summer and winter. Median hourly averages and standard error bars at local hour are plotted. A bias correction of 1 pH unit is applied due to not considering ammonia partitioning.

Although organics are less hygroscopic than ammonium sulfate, a large fraction of the $PM_{2.5}$ ($\sim 70\%$) was organic, making W_o contributions important. Cerully et al. (2014) showed that, of the organic factors associated with W_o , MO-OOA (more-oxidized oxygenated organic aerosol, also referred to as LVOOA: low-volatility oxygenated organic aerosol) and isoprene-OA (isoprene-derived organic aerosol) were twice as hygroscopic as LO-OOA (less-oxidized oxygenated organic aerosol, also referred to as SVOOA: semi-volatile oxygenated organic aerosol). The LWC associated with MO-OOA and isoprene-OA accounts for ~ 60 and $\sim 30\%$ of total W_o in the daytime, respectively.

The effect of particle water on pH can also be delineated. pH calculated just by W_i alone will be affected by an underestimation of particle water, resulting in a slightly lower pH (Fig. 13). W_o is on average 29 to 39% of total water at all sites; as a result pH increases by 0.15 to 0.23 units when W_o is included. Independent of the pH range, a 29 to 39% W_o fraction always increases pH by 0.15 to 0.23 due to the logarithmic nature of pH. The effect of W_o on pH can be simply denoted as $\log_{10}(1 - \varepsilon_{W_o})$. For example, when ε_{W_o} is 90%, it shifts pH up by 1 unit. pH based on W_i is highly

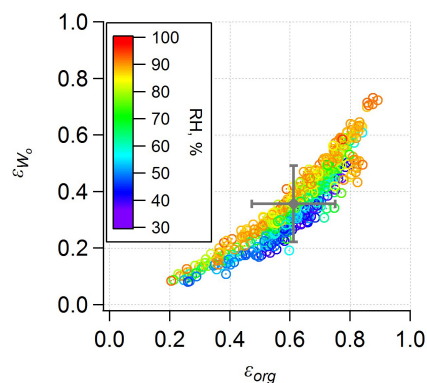


Figure 12. W_o mass fraction (ε_{W_o}) plotted versus organic mass fraction at CTR (SOAS). Overall study mean and standard deviation is also shown. $\varepsilon_{Org} = 61 \pm 14\%$ and $\varepsilon_{W_o} = 36 \pm 14\%$.

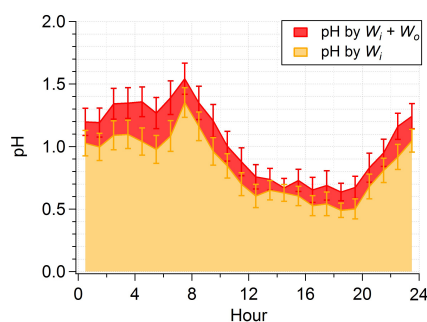


Figure 13. CTR (SOAS) pH diurnal profiles based on total predicted water and W_i , respectively. Median hourly averages and standard error bars at local hour are plotted.

correlated with pH for total water ($W_i + W_o$) (slope = 0.94, intercept = -0.14 , $R^2 = 0.97$). This indicates that, if organic mass and κ_{Org} are not available, ISORROPIA-II run with only ion data will give a reasonable estimate of pH, since both H_{air}^+ and W_i are outputs of ISORROPIA-II, while W_o is predicted based on organic mass and κ_{Org} . Accurate temperature and RH are still necessary inputs, especially when RH is high.

4.4 Overall implications of low pH

Highly acidic aerosols throughout the southeast during all seasons will affect a variety of processes. For example, aerosol acidity strongly shifts the partitioning of $HNO_3(g)$ to the gas phase, resulting in low nitrate aerosol levels in the southeast during summer (the higher summertime temperature also plays a secondary role). Aerosol acidity also impacts the gas–particle partitioning of semi-volatile organic acids. Note that organic acids are not considered in our model; under these acidic conditions (pH = 1) their contributions to the H_{air}^+ (hence pH) are expected to be negligible. Because the pK_a ($pK_a = -\log_{10}K_a$, with K_a referring to acid dissociation constant) of trace organic acids is > 2 (e.g., pK_a of formic acid, one of the strongest organic acids, is 3.75;

Bacarella et al., 1955), low pH prevents dissociation of the organic acids. Since H^+ is involved in aqueous-phase reactions, low pH can affect reaction rates by providing protons. Investigators have found that isoprene-OA formation is acid-catalyzed and sulfuric acid participates in the reaction as a proton donor in chamber studies (Surratt et al., 2007). However, aerosol acidity appears not to be a limiting factor for isoprene-OA formation in the southeastern USA, owing to the consistently very low pH (Karambelas et al., 2014; Xu et al., 2015). Finally, low pH can affect the solubility of trace metals (e.g., mineral dust) such as Fe and Cu, which possibly increases the toxicity of the redox metals (Ghio et al., 2012; Verma et al., 2014) and may also have a long-term effect on nutrient distributions in the region (Meskhidze et al., 2003; Meskhidze et al., 2005; Nenes et al., 2011; Ito and Xu, 2014).

5 Conclusions

Particle pH is important and difficult to measure directly. However, the commonly used pH proxies of ion balances and NH_4^+/SO_4^{2-} molar ratios do not necessarily correlate with pH. Therefore, predicting pH is the best method to analyze particle acidity. By combining several models we present a comprehensive prediction method to calculate pH and include an uncertainty analysis. ISORROPIA-II is applied to calculate the concentration of H_{air}^+ and W_i from inorganic aerosol measurements, and CCN activity is used to predict W_o . The adjoint model of ISORROPIA, ANISORROPIA, is applied to determine sensitivities, which are used for propagating the measurement uncertainties to pH. We find that W_o should be included when predicting particle LWC when organic loadings are high (such as in the southeastern US). However, the pH prediction is not highly sensitive to W_o , unless W_o mass fraction to the total particle water is close to 1. Thus, in most cases particle pH can be predicted fairly accurately with just measurements of inorganic species and ISORROPIA-II. However, constraining ISORROPIA-II with gas-phase species, such as $NH_3(g)$, as done in this work (or $HNO_3(g)$), is highly recommended, along with running ISORROPIA-II in the forward mode. ISORROPIA-II does not consider organic acids, but at the low pHs of this study they do not contribute protons. However, when pH approaches 7, the dissociation of organic acids cannot be neglected. Finally, the model was validated through comparing predicted to measured liquid water ($W_i + W_o$ to $f(RH)_{water}$) and predicted to measured $NH_3(g)$ concentrations.

On average, for the SOAS and SCAPE field studies, particle water associated with the $PM_{2.5}$ organic species (W_o) accounted for a significant fraction of total LWC, with a mean of 35 % (± 3 % SD) indicating the importance of organic hygroscopic properties to aqueous-phase chemistry and radiative forcing in the southeast US. Although organics are less

hygroscopic than sulfate and ammonium, the larger mass fraction of organics than inorganics promotes W_o uptake. Predicted LWC was compared to LWC determined from ambient versus dry light scattering coefficients and a TEOM measurement of dry $PM_{2.5}$ mass. In SOAS, the sum of W_i and W_o was highly correlated and in close agreement with the measured LWC (slope = 0.91, $R^2 = 0.75$). LWC showed a clear diurnal pattern, with a continuous increase at night (median of $10 \mu g m^{-3}$ at 07:30), reaching a distinct peak when RH reached a maximum near 90 % just after sunrise during the period of lowest daily temperature, followed by a rapid decrease and lower values during the day (median of $2 \mu g m^{-3}$ at 14:30).

In the southeastern USA, pH normally varied from 0.5 to 2 in the summer and 1 to 3 in the winter, indicating that the aerosol was highly acidic throughout the year. The minimum and maximum pH were -0.94 and 2.2 at CTR, respectively, and varied from a nighttime average of 1.5 to daytime average of 0.6, mostly attributable to diurnal variation in RH and temperature. Mean NH_4^+/SO_4^{2-} molar ratios were 1.4 ± 0.5 (SD), and roughly half the ammonia was in the gas phase ($NH_3(g)/(NH_3(g) + NH_4^+) = 41 \pm 16$ %, mean \pm SD). pH at other sites in the southeast (SCAPE study) was estimated based on a limited data set at an estimated uncertainty of 9–49 % and a systematic bias of -1 since $NH_3(g)$ is not included in the thermodynamic model run in the forward mode. pH can still be predicted with only aerosol measurements, but an adjustment of 1 unit pH increase is recommended for the southeastern US. pH has a diurnal trend that follows LWC, higher (less acidic) at night and lower (more acidic) during the day. pH was also generally higher in the winter (~ 2) than summer (~ 1). These low pHs have significant implications for gas–aerosol partitioning, acid-catalyzed reactions including isoprene-OA formation, and trace metal mobilization.

The Supplement related to this article is available online at doi:10.5194/acp-15-5211-2015-supplement.

Acknowledgements. This work was supported by the NSF under grant number 1242258 as part of the SOAS campaign. GIT SOAS researchers were also supported by a US EPA STAR grant R835410 and NOAA CPO Award NA10OAR4310102. Measurements at other sites in the southeast were part of the EPA-supported SCAPE Clean Air Center, made possible through US EPA grant R834799. The content of this publication are solely the responsibility of the grantee and do not necessarily represent the official views of the US EPA. Further, the US EPA does not endorse the purchase of any commercial products or services mentioned in the publication. S. L. Capps was supported by an appointment to the Research Participation Program at the Office of Research and Development, US EPA, administered by ORISE. A. Nenes acknowledges support from a Georgia Power Faculty Scholar Chair and a Cullen-Peck Faculty Fellowship from the Georgia Institute of Technology. We

would also like to thank Richard Moore from NASA Langley for valuable suggestions and discussions. S.-H. Lee acknowledges funding support from NSF (AGS-1241498). A. Bougiatioti acknowledges support within the framework of the Action Supporting Postdoctoral Researchers of the Operational Program “Education and Lifelong Learning” (Action’s Beneficiary: General Secretariat for Research and Technology) and is co-financed by the European Social Fund (ESF) and the Greek state. We wish to thank the Southeastern Aerosol Research and Characterization (SEARCH) personnel for their many contributions supporting the field deployments.

Edited by: B. Ervens

References

- Bacarella, A. L., Grunwald, E., Marshall, H. P., and Purlee, E. L.: The Potentiometric Measurement of Acid Dissociation Constants and pH in the System Methanol-Water. pK_a Values for Carboxylic Acids and Anilinium Ions, *J. Org. Chem.*, 20, 747–762, doi:10.1021/Jo01124a007, 1955.
- Bertram, A. K., Martin, S. T., Hanna, S. J., Smith, M. L., Bodsworth, A., Chen, Q., Kuwata, M., Liu, A., You, Y., and Zorn, S. R.: Predicting the relative humidities of liquid-liquid phase separation, efflorescence, and deliquescence of mixed particles of ammonium sulfate, organic material, and water using the organic-to-sulfate mass ratio of the particle and the oxygen-to-carbon elemental ratio of the organic component, *Atmos. Chem. Phys.*, 11, 10995–11006, doi:10.5194/acp-11-10995-2011, 2011.
- Canagaratna, M. R., Jayne, J. T., Jimenez, J. L., Allan, J. D., Alfarra, M. R., Zhang, Q., Onasch, T. B., Drewnick, F., Coe, H., Middlebrook, A., Delia, A., Williams, L. R., Trimborn, A. M., Northway, M. J., DeCarlo, P. F., Kolb, C. E., Davidovits, P., and Worsnop, D. R.: Chemical and microphysical characterization of ambient aerosols with the aerodyne aerosol mass spectrometer, *Mass Spectrom. Rev.*, 26, 185–222, doi:10.1002/mas.20115, 2007.
- Capps, S. L., Henze, D. K., Hakami, A., Russell, A. G., and Nenes, A.: ANISORROPIA: the adjoint of the aerosol thermodynamic model ISORROPIA, *Atmos. Chem. Phys.*, 12, 527–543, doi:10.5194/acp-12-527-2012, 2012.
- Carlton, A. G. and Turpin, B. J.: Particle partitioning potential of organic compounds is highest in the Eastern US and driven by anthropogenic water, *Atmos. Chem. Phys.*, 13, 10203–10214, doi:10.5194/acp-13-10203-2013, 2013.
- Carrico, C. M., Rood, M. J., and Ogren, J. A.: Aerosol light scattering properties at Cape Grim, Tasmania, during the First Aerosol Characterization Experiment (ACE 1), *J. Geophys. Res.*, 103, 16565, doi:10.1029/98jd00685, 1998.
- Carrico, C. M., Rood, M. J., Ogren, J. A., Neususs, C., Wiedensohler, A., and Heintzenberg, J.: Aerosol optical properties at Sagres, Portugal during ACE-2, *Tellus B*, 52, 694–715, doi:10.1034/j.1600-0889.2000.00049.x, 2000.
- Cerully, K. M., Bougiatioti, A., Hite Jr., J. R., Guo, H., Xu, L., Ng, N. L., Weber, R., and Nenes, A.: On the link between hygroscopicity, volatility, and oxidation state of ambient and water-soluble aerosol in the Southeastern United States, *Atmos. Chem. Phys. Discuss.*, 14, 30835–30877, doi:10.5194/acpd-14-30835-2014, 2014.
- Clegg, S. L., Brimblecombe, P., and Wexler, A. S.: Thermodynamic model of the system $H^+ - NH_4^+ - SO_4^{2-} - NO_3^- - H_2O$ at tropospheric temperatures, *J. Phys. Chem. A*, 102, 2137–2154, doi:10.1021/Jp973042r, 1998.
- Czochke, N. M. and Jang, M.: Acidity effects on the formation of α -pinene ozone SOA in the presence of inorganic seed, *Atmos. Environ.*, 40, 4370–4380, doi:10.1016/j.atmosenv.2006.03.030, 2006.
- DeCarlo, P. F., Kimmel, J. R., Trimborn, A., Northway, M. J., Jayne, J. T., Aiken, A. C., Gonin, M., Fuhrer, K., Horvath, T., Docherty, K. S., Worsnop, D. R., and Jimenez, J. L.: Field-deployable, high-resolution, time-of-flight aerosol mass spectrometer, *Anal. Chem.*, 78, 8281–8289, doi:10.1021/ac061249n, 2006.
- Eddingsaas, N. C., VanderVelde, D. G., and Wennberg, P. O.: Kinetics and Products of the Acid-Catalyzed Ring-Opening of Atmospherically Relevant Butyl Epoxy Alcohols, *J. Phys. Chem. A*, 114, 8106–8113, doi:10.1021/Jp103907c, 2010.
- Edney, E. O., Kleindienst, T. E., Jaoui, M., Lewandowski, M., Offenberg, J. H., Wang, W., and Claeys, M.: Formation of 2-methyl tetrols and 2-methylglyceric acid in secondary organic aerosol from laboratory irradiated isoprene/ NO_x / SO_2 /air mixtures and their detection in ambient $PM_{2.5}$ samples collected in the eastern United States, *Atmos. Environ.*, 39, 5281–5289, doi:10.1016/j.atmosenv.2005.05.031, 2005.
- Engelhart, G. J., Asa-Awuku, A., Nenes, A., and Pandis, S. N.: CCN activity and droplet growth kinetics of fresh and aged monoterpene secondary organic aerosol, *Atmos. Chem. Phys. Discuss.*, 8, 95–135, doi:10.5194/acpd-8-95-2008, 2008.
- Ervens, B., Turpin, B. J., and Weber, R. J.: Secondary organic aerosol formation in cloud droplets and aqueous particles (aq-SOA): a review of laboratory, field and model studies, *Atmos. Chem. Phys. Discuss.*, 11, 22301–22383, doi:10.5194/acpd-11-22301-2011, 2011.
- Fountoukis, C. and Nenes, A.: ISORROPIA II: a computationally efficient thermodynamic equilibrium model for $K^+ - Ca^{2+} - Mg^{2+} - NH_4^+ - Na^+ - SO_4^{2-} - NO_3^- - Cl^- - H_2O$ aerosols, *Atmos. Chem. Phys.*, 7, 4639–4659, doi:10.5194/acp-7-4639-2007, 2007.
- Fountoukis, C., Nenes, A., Sullivan, A., Weber, R., Van Reken, T., Fischer, M., Matías, E., Moya, M., Farmer, D., and Cohen, R. C.: Thermodynamic characterization of Mexico City aerosol during MILAGRO 2006, *Atmos. Chem. Phys.*, 9, 2141–2156, doi:10.5194/acp-9-2141-2009, 2009.
- Frosch, M., Bilde, M., DeCarlo, P. F., Jurányi, Z., Tritscher, T., Dommen, J., Donahue, N. M., Gysel, M., Weingartner, E., and Baltensperger, U.: Relating cloud condensation nuclei activity and oxidation level of α -pinene secondary organic aerosols, *J. Geophys. Res.-Atmos.*, 116, doi:10.1029/2011jd016401, 2011.
- Gao, S., Keywood, M., Ng, N. L., Surratt, J., Varutbangkul, V., Bahreini, R., Flagan, R. C., and Seinfeld, J. H.: Low-molecular-weight and oligomeric components in secondary organic aerosol from the ozonolysis of cycloalkenes and alpha-pinene, *J. Phys. Chem. A*, 108, 10147–10164, doi:10.1021/Jp047466e, 2004.
- Ghio, A. J., Carraway, M. S., and Madden, M. C.: Composition of air pollution particles and oxidative stress in cells, tissues, and living systems, *J. Toxicol. Env. Heal. B*, 15, 1–21, doi:10.1080/10937404.2012.632359, 2012.

- Hansen, D. A., Edgerton, E. S., Hartsell, B. E., Jansen, J. J., Kandasamy, N., Hidy, G. M., and Blanchard, C. L.: The Southeastern Aerosol Research and Characterization Study: Part 1 – Overview, *J. Air Waste Manage.*, 53, 1460–1471, doi:10.1080/10473289.2003.10466318, 2003.
- Hansen, D. A., Edgerton, E., Hartsell, B., Jansen, J., Burge, H., Koutrakis, P., Rogers, C., Suh, H., Chow, J., Zielinska, B., McMurry, P., Mulholland, J., Russell, A., and Rasmussen, R.: Air Quality Measurements for the Aerosol Research and Inhalation Epidemiology Study, *J. Air Waste Manage.*, 56, 1445–1458, doi:10.1080/10473289.2006.10464549, 2006.
- Hennigan, C. J., Bergin, M. H., Dibb, J. E., and Weber, R. J.: Enhanced secondary organic aerosol formation due to water uptake by fine particles, *Geophys. Res. Lett.*, 35, L18801, doi:10.1029/2008gl035046, 2008.
- Hennigan, C. J., Izumi, J., Sullivan, A. P., Weber, R. J., and Nenes, A.: A critical evaluation of proxy methods used to estimate the acidity of atmospheric particles, *Atmos. Chem. Phys.*, 15, 2775–2790, doi:10.5194/acp-15-2775-2015, 2015.
- Hildebrandt Ruiz, L., Paciga, A. L., Cerully, K., Nenes, A., Donahue, N. M., and Pandis, S. N.: Aging of secondary organic aerosol from small aromatic VOCs: changes in chemical composition, mass yield, volatility and hygroscopicity, *Atmos. Chem. Phys. Discuss.*, 14, 31441–31481, doi:10.5194/acpd-14-31441-2014, 2014.
- Inuma, Y., Böge, O., Gnauk, T., and Herrmann, H.: Aerosol-chamber study of the α -pinene/O₃ reaction: influence of particle acidity on aerosol yields and products, *Atmos. Environ.*, 38, 761–773, doi:10.1016/j.atmosenv.2003.10.015, 2004.
- IPCC: Climate Change 2013: The Physical Science Basis. Contribution of Working Group I to the Fifth Assessment Report of the Intergovernmental Panel on Climate Change, Cambridge University Press, Cambridge, United Kingdom and New York, NY, USA, 1535 pp., 2013.
- Ito, A. and Xu, L.: Response of acid mobilization of iron-containing mineral dust to improvement of air quality projected in the future, *Atmos. Chem. Phys.*, 14, 3441–3459, doi:10.5194/acp-14-3441-2014, 2014.
- Jang, M., Czoschke, N. M., Lee, S., and Kamens, R. M.: Heterogeneous atmospheric aerosol production by acid-catalyzed particle-phase reactions, *Science*, 298, 814–817, doi:10.1126/science.1075798, 2002.
- Karambelas, A., Pye, H. O. T., Budisulistiorini, S. H., Surratt, J. D., and Pinder, R. W.: Contribution of Isoprene Epoxydiol to Urban Organic Aerosol: Evidence from Modeling and Measurements, *Environ. Sci. Technol. Lett.*, 1, 278–283, doi:10.1021/ez5001353, 2014.
- Kim, J., Yoon, S.-C., Jefferson, A., and Kim, S.-W.: Aerosol hygroscopic properties during Asian dust, pollution, and biomass burning episodes at Gosan, Korea in April 2001, *Atmos. Environ.*, 40, 1550–1560, doi:10.1016/j.atmosenv.2005.10.044, 2006.
- King, S. M., Rosenoern, T., Shilling, J. E., Chen, Q., and Martin, S. T.: Cloud condensation nucleus activity of secondary organic aerosol particles mixed with sulfate, *Geophys. Res. Lett.*, 34, L24806, doi:10.1029/2007gl030390, 2007.
- Kleindienst, T. E., Edney, E. O., Lewandowski, M., Offenberg, J. H., and Jaoui, M.: Secondary organic carbon and aerosol yields from the irradiations of isoprene and α -pinene in the presence of NO_x and SO₂, *Environ. Sci. Technol.*, 40, 3807–3812, doi:10.1021/Es052446r, 2006.
- Kotchenruther, R. A. and Hobbs, P. V.: Humidification factors of aerosols from biomass burning in Brazil, *J. Geophys. Res.*, 103, 32081, doi:10.1029/98jd00340, 1998.
- Kuwata, M., Zorn, S. R., and Martin, S. T.: Using elemental ratios to predict the density of organic material composed of carbon, hydrogen, and oxygen, *Environ. Sci. Technol.*, 46, 787–794, doi:10.1021/es202525q, 2012.
- Lance, S., Nenes, A., Medina, J., and Smith, J. N.: Mapping the Operation of the DMT Continuous Flow CCN Counter, *Aerosol Sci. Technol.*, 40, 242–254, doi:10.1080/02786820500543290, 2006.
- Liao, H. and Seinfeld, J. H.: Global impacts of gas-phase chemistry-aerosol interactions on direct radiative forcing by anthropogenic aerosols and ozone, *J. Geophys. Res.-Atmos.*, 110, D18208, doi:10.1029/2005jd005907, 2005.
- Liu, J., Zhang, X., Parker, E. T., Veres, P. R., Roberts, J. M., de Gouw, J. A., Hayes, P. L., Jimenez, J. L., Murphy, J. G., Ellis, R. A., Huey, L. G., and Weber, R. J.: On the gas-particle partitioning of soluble organic aerosol in two urban atmospheres with contrasting emissions: 2. Gas and particle phase formic acid, *J. Geophys. Res.*, 117, D00V21, doi:10.1029/2012jd017912, 2012.
- Magi, B. I. and Hobbs, P. V.: Effects of humidity on aerosols in southern Africa during the biomass burning season, *J. Geophys. Res.*, 108, 8495, doi:10.1029/2002jd002144, 2003.
- Malm, W. C. and Day, D. E.: Estimates of aerosol species scattering characteristics as a function of relative humidity, *Atmos. Environ.*, 35, 2845–2860, doi:10.1016/S1352-2310(01)00077-2, 2001.
- Meskhidze, N., Chameides, W. L., Nenes, A., and Chen, G.: Iron mobilization in mineral dust: Can anthropogenic SO₂ emissions affect ocean productivity?, *Geophys. Res. Lett.*, 30, 2085, doi:10.1029/2003gl018035, 2003.
- Meskhidze, N., Chameides, W. L., and Nenes, A.: Dust and pollution: A recipe for enhanced ocean fertilization?, *J. Geophys. Res.*, 110, D03301, doi:10.1029/2004jd005082, 2005.
- Mitchell, R. M., Campbell, S. K., Qin, Y., and Gras, J. L.: Performance Characteristics of Integrating Nephelometers in the Australian Outback, *J. Atmos. Ocean. Tech.*, 26, 984–995, doi:10.1175/2008jtecha1187.1, 2009.
- Nemesure, S., Wagener, R., and Schwartz, S. E.: Direct shortwave forcing of climate by the anthropogenic sulfate aerosol: Sensitivity to particle size, composition, and relative humidity, *J. Geophys. Res.-Atmos.*, 100, 26105–26116, doi:10.1029/95jd02897, 1995.
- Nenes, A., Pandis, S. N., and Pilinis, C.: ISORROPIA: A new thermodynamic equilibrium model for multiphase multi-component inorganic aerosols, *Aquat. Geochem.*, 4, 123–152, doi:10.1023/A:1009604003981, 1998.
- Nenes, A., Krom, M. D., Mihalopoulos, N., Van Cappellen, P., Shi, Z., Bougiatioti, A., Zarrmpas, P., and Herut, B.: Atmospheric acidification of mineral aerosols: a source of bioavailable phosphorus for the oceans, *Atmos. Chem. Phys.*, 11, 6265–6272, doi:10.5194/acp-11-6265-2011, 2011.
- Nguyen, T. B., Coggon, M. M., Flagan, R. C., and Seinfeld, J. H.: Reactive uptake and photo-Fenton oxidation of glycolaldehyde in aerosol liquid water, *Environ. Sci. Technol.*, 47, 4307–4316, doi:10.1021/es400538j, 2013.

- Nguyen, T. K. V., Petters, M. D., Suda, S. R., Guo, H., Weber, R. J., and Carlton, A. G.: Trends in particle-phase liquid water during the Southern Oxidant and Aerosol Study, *Atmos. Chem. Phys.*, 14, 10911–10930, doi:10.5194/acp-14-10911-2014, 2014.
- Nowak, J. B., Huey, L. G., Russell, A. G., Tian, D., Neuman, J. A., Orsini, D., Sjostedt, S. J., Sullivan, A. P., Tanner, D. J., Weber, R. J., Nenes, A., Edgerton, E., and Fehsenfeld, F. C.: Analysis of urban gas phase ammonia measurements from the 2002 Atlanta Aerosol Nucleation and Real-Time Characterization Experiment (ANARChE), *J. Geophys. Res.*, 111, D17308, doi:10.1029/2006jd007113, 2006.
- Orsini, D. A., Ma, Y., Sullivan, A., Sierau, B., Baumann, K., and Weber, R. J.: Refinements to the particle-into-liquid sampler (PILS) for ground and airborne measurements of water soluble aerosol composition, *Atmos. Environ.*, 37, 1243–1259, doi:10.1016/s1352-2310(02)01015-4, 2003.
- Pathak, R. K., Wang, T., Ho, K. F., and Lee, S. C.: Characteristics of summertime PM_{2.5} organic and elemental carbon in four major Chinese cities: Implications of high acidity for water-soluble organic carbon (WSOC), *Atmos. Environ.*, 45, 318–325, doi:10.1016/j.atmosenv.2010.10.021, 2011.
- Petters, M. D. and Kreidenweis, S. M.: A single parameter representation of hygroscopic growth and cloud condensation nucleus activity, *Atmos. Chem. Phys.*, 7, 1961–1971, doi:10.5194/acp-7-1961-2007, 2007.
- Pilinis, C., Pandis, S. N., and Seinfeld, J. H.: Sensitivity of Direct Climate Forcing by Atmospheric Aerosols to Aerosol-Size and Composition, *J. Geophys. Res.-Atmos.*, 100, 18739–18754, doi:10.1029/95jd02119, 1995.
- Pye, H. O., Pinder, R. W., Piletic, I. R., Xie, Y., Capps, S. L., Lin, Y. H., Surratt, J. D., Zhang, Z., Gold, A., Luecken, D. J., Hutzell, W. T., Jaoui, M., Offenberg, J. H., Kleindienst, T. E., Lewandowski, M., and Edney, E. O.: Epoxide pathways improve model predictions of isoprene markers and reveal key role of acidity in aerosol formation, *Environ. Sci. Technol.*, 47, 11056–11064, doi:10.1021/es402106h, 2013.
- Roberts, G. C. and Nenes, A.: A Continuous-Flow Streamwise Thermal-Gradient CCN Chamber for Atmospheric Measurements, *Aerosol Sci. Technol.*, 39, 206–221, doi:10.1080/027868290913988, 2005.
- Seinfeld, J. H. and Pandis, S. N.: *Atmospheric Chemistry and Physics: from Air Pollution to Climate Change 2nd Edn.*, John Wiley & Sons, Inc., Hoboken, New Jersey, 2006.
- Sheridan, P. J., Jefferson, A., and Ogren, J. A.: Spatial variability of submicrometer aerosol radiative properties over the Indian Ocean during INDOEX, *J. Geophys. Res.*, 107, 8011, doi:10.1029/2000jd000166, 2002.
- Sloane, C. S., Watson, J., Chow, J., Pritchett, L., and Richards, L. W.: Size-Segregated Fine Particle Measurements by Chemical-Species and Their Impact on Visibility Impairment in Denver, *Atmos. Environ. A-Gen.*, 25, 1013–1024, doi:10.1016/0960-1686(91)90143-U, 1991.
- Song, M., Marcolli, C., Krieger, U. K., Zuend, A., and Peter, T.: Liquid-liquid phase separation and morphology of internally mixed dicarboxylic acids/ammonium sulfate/water particles, *Atmos. Chem. Phys.*, 12, 2691–2712, doi:10.5194/acp-12-2691-2012, 2012.
- Song, M., Liu, P. F., Hanna, S. J., Martin, S. T., and Bertram, A. K.: Relative humidity-dependent viscosities of isoprene-derived secondary organic material and atmospheric implications for isoprene-dominant forests, *Atmos. Chem. Phys. Discuss.*, 15, 1131–1169, doi:10.5194/acpd-15-1131-2015, 2015.
- Sorooshian, A., Hersey, S., Brechtel, F. J., Corless, A., Flagan, R. C., and Seinfeld, J. H.: Rapid, Size-Resolved Aerosol Hygroscopic Growth Measurements: Differential Aerosol Sizing and Hygroscopicity Spectrometer Probe (DASH-SP), *Aerosol Sci. Technol.*, 42, 445–464, doi:10.1080/02786820802178506, 2008.
- Stein, S. W., Turpin, B. J., Cai, X. P., Huang, C. P. F., and McMurry, P. H.: Measurements of Relative Humidity-Dependent Bounce and Density for Atmospheric Particles Using the DMA-Impactor Technique, *Atmos. Environ.*, 28, 1739–1746, doi:10.1016/1352-2310(94)90136-8, 1994.
- Stokes, R. H. and Robinson, R. A.: Interactions in Aqueous Nonelectrolyte Solutions. I. Solute-Solvent Equilibria, *J. Phys. Chem.*, 70, 2126–2130, doi:10.1021/J100879a010, 1966.
- Surratt, J. D., Lewandowski, M., Offenberg, J. H., Jaoui, M., Kleindienst, T. E., Edney, E. O., and Seinfeld, J. H.: Effect of acidity on secondary organic aerosol formation from isoprene, *Environ. Sci. Technol.*, 41, 5363–5369, doi:10.1021/es0704176, 2007.
- Surratt, J. D., Chan, A. W., Eddingsaas, N. C., Chan, M., Loza, C. L., Kwan, A. J., Hersey, S. P., Flagan, R. C., Wennberg, P. O., and Seinfeld, J. H.: Reactive intermediates revealed in secondary organic aerosol formation from isoprene, *P. Natl. Acad. Sci. USA*, 107, 6640–6645, doi:10.1073/pnas.0911114107, 2010.
- Tang, I. N.: Phase transformation and growth of aerosol particles composed of mixed salts, *J. Aerosol Sci.*, 7, 361–371, doi:10.1016/0021-8502(76)90022-7, 1976.
- Tang, I. N. and Munkelwitz, H. R.: Composition and Temperature-Dependence of the Deliquescence Properties of Hygroscopic Aerosols, *Atmos. Environ. A-Gen.*, 27, 467–473, doi:10.1016/0960-1686(93)90204-C, 1993.
- Tanner, R. L., Olszyna, K. J., Edgerton, E. S., Knipping, E., and Shaw, S. L.: Searching for evidence of acid-catalyzed enhancement of secondary organic aerosol formation using ambient aerosol data, *Atmos. Environ.*, 43, 3440–3444, doi:10.1016/j.atmosenv.2009.03.045, 2009.
- Tolocka, M. P., Jang, M., Ginter, J. M., Cox, F. J., Kamens, R. M., and Johnston, M. V.: Formation of oligomers in secondary organic aerosol, *Environ. Sci. Technol.*, 38, 1428–1434, doi:10.1021/es035030r, 2004.
- Turpin, B. J. and Lim, H.-J.: Species Contributions to PM_{2.5} Mass Concentrations: Revisiting Common Assumptions for Estimating Organic Mass, *Aerosol Sci. Technol.*, 35, 602–610, doi:10.1080/02786820119445, 2001.
- Verma, V., Fang, T., Guo, H., King, L., Bates, J. T., Peltier, R. E., Edgerton, E., Russell, A. G., and Weber, R. J.: Reactive oxygen species associated with water-soluble PM_{2.5} in the southeastern United States: spatiotemporal trends and source apportionment, *Atmos. Chem. Phys.*, 14, 12915–12930, doi:10.5194/acp-14-12915-2014, 2014.
- Villani, P., Sellegri, K., Monier, M., and Laj, P.: Influence of semi-volatile species on particle hygroscopic growth, *Atmos. Environ.*, 79, 129–137, doi:10.1016/j.atmosenv.2013.05.069, 2013.
- Wexler, A. S. and Seinfeld, J. H.: Second-generation inorganic aerosol model, *Atmos. Environ. A-Gen.*, 25, 2731–2748, doi:10.1016/0960-1686(91)90203-J, 1991.
- Xu, L., Guo, H., Boyd, C. M., Klein, M., Bougiatioti, A., Cerully, K. M., Hite, J. R., Isaacman-VanWertz, G., Kreisberg, N. M., Knote,

- C., Olson, K., Koss, A., Goldstein, A. H., Hering, S. V., de Gouw, J., Baumann, K., Lee, S.-H., Nenes, A., Weber, R. J., and Ng, N. L.: Effects of anthropogenic emissions on aerosol formation from isoprene and monoterpenes in the southeastern United States, *P. Natl. Acad. Sci.*, 112, 37–42, doi:10.1073/pnas.1417609112, 2015.
- Yin, L., Niu, Z., Chen, X., Chen, J., Zhang, F., and Xu, L.: Characteristics of water-soluble inorganic ions in PM_{2.5} and PM_{2.5–10} in the coastal urban agglomeration along the Western Taiwan Strait Region, China, *Environ. Sci. Pollut. R.*, 21, 5141–5156, doi:10.1007/s11356-013-2134-7, 2014.
- You, Y., Renbaum-Wolff, L., Carreras-Sospedra, M., Hanna, S. J., Hiranuma, N., Kamal, S., Smith, M. L., Zhang, X., Weber, R. J., Shilling, J. E., Dabdub, D., Martin, S. T., and Bertram, A. K.: Images reveal that atmospheric particles can undergo liquid-liquid phase separations, *P. Natl. Acad. Sci. USA*, 109, 13188–13193, doi:10.1073/pnas.1206414109, 2012.
- You, Y., Renbaum-Wolff, L., and Bertram, A. K.: Liquid-liquid phase separation in particles containing organics mixed with ammonium sulfate, ammonium bisulfate, ammonium nitrate or sodium chloride, *Atmos. Chem. Phys.*, 13, 11723–11734, doi:10.5194/acp-13-11723-2013, 2013.
- You, Y., Kanawade, V. P., de Gouw, J. A., Guenther, A. B., Madronich, S., Sierra-Hernández, M. R., Lawler, M., Smith, J. N., Takahama, S., Ruggeri, G., Koss, A., Olson, K., Baumann, K., Weber, R. J., Nenes, A., Guo, H., Edgerton, E. S., Porcelli, L., Brune, W. H., Goldstein, A. H., and Lee, S.-H.: Atmospheric amines and ammonia measured with a chemical ionization mass spectrometer (CIMS), *Atmos. Chem. Phys.*, 14, 12181–12194, doi:10.5194/acp-14-12181-2014, 2014.
- Zdanovskii, A. B.: *Trudy Sol'nyanoi Laboratorii Akad. Nauk SSSR*, 2, 1936.
- Zhang, X., Liu, Z., Hecobian, A., Zheng, M., Frank, N. H., Edgerton, E. S., and Weber, R. J.: Spatial and seasonal variations of fine particle water-soluble organic carbon (WSOC) over the southeastern United States: implications for secondary organic aerosol formation, *Atmos. Chem. Phys.*, 12, 6593–6607, doi:10.5194/acp-12-6593-2012, 2012.
- Zuend, A. and Seinfeld, J. H.: Modeling the gas-particle partitioning of secondary organic aerosol: the importance of liquid-liquid phase separation, *Atmos. Chem. Phys.*, 12, 3857–3882, doi:10.5194/acp-12-3857-2012, 2012.
- Zuend, A., Marcolli, C., Peter, T., and Seinfeld, J. H.: Computation of liquid-liquid equilibria and phase stabilities: implications for RH-dependent gas/particle partitioning of organic-inorganic aerosols, *Atmos. Chem. Phys.*, 10, 7795–7820, doi:10.5194/acp-10-7795-2010, 2010.